Formation, Dynamics and Statistics of Patterns

Volume 1

Editors

Kyozi Kawasaki
Kyushu University

Masuo Suzuki
University of Tokyo

Akira Onuki
Kyoto University

World Scientific (1990)

[45]

Simulating Physics with Coupled Map Lattices

Pattern Dynamics, Information Flow, and Thermodynamics of Spatiotemporal Chaos

Kunihiko Kaneko
Center for Nonlinear Studies,
Los Alamos National Laboratory,
Los Alamos, NM 87545
and
Institute of Physics,
College of Arts and Sciences,
University of Tokyo,
Komaba, Meguro-ku, Tokyo 153, Japan

Contents

1 Introduction — Why Coupled Map Lattices? 3

2 Pattern Dynamics in a 1-dimensional Lattice 5
2.1 Global phase diagram 5
Spatial power spectra 5
Temporal power spectra 9
Lyapunov analysis 9
2.2 Frozen random pattern 13
2.3 Pattern selection and suppression of chaos 13
2.4 Selection of zigzag pattern and chaotic diffusion of defects 14
2.5 Spatiotemporal intermittency transition: Defect turbulence and pattern competition intermittency 16
(I)Defect turbulence 16
(II)Selective flicker noise 16
(III)Quantitative analysis of pattern dynamics 18
(IV)Pattern competition intermittency 21
2.6 Fully developed turbulence 22
2.7 Summing Up... 22

3 Pattern Dynamics in a 2-dimensional Lattice 23
3.1 Checkerboard pattern selection, chaotic string, and spatiotemporal intermittency 25
3.2 Selection of larger patterns 25
3.3 Absence of a frozen pattern for stronger coupling and extension of Pierls' argument 28

4 Open Flow Models 29

5 Information Flow 32

6 Thermodynamics 34

7 Mean-field Type Model 35

8 Simulating Science with Coupled Map Lattices 35
8.1 Pattern formation (spinodal decomposition) . . . 36
8.2 Other pattern formation problems . . . 36
8.3 Crystal growth . . . 37
8.4 Excitable media . . . 37
8.5 Dripping handrail and boiling chaos . . . 39
8.6 Designing fluid dynamics with CML? . . . 39
8.7 Neural networks . . . 43
8.8 Josephson junction, CDW, ... and coupled circle lattice . . . 44
8.9 Other applications . . . 44
8.10 Experimental observation of spatiotemporal chaos . . . 44
to conclude ...? . . . 45

9 Appendix: Quantifiers in Spatiotemporal Chaos (in alphabetical order) 46
Co-moving Lyapunov spectra . . . 46
Co-moving mutual information flow . . . 46
Dimension density . . . 46
Dynamical form factor (Spatiotemporal power spectra) . . . 47
Kolmogorov-Sinai entropy density . . . 47
Lyapunov spectra . . . 47
Mutual information in spacetime . . . 48
Pattern dynamics quantifiers . . . 48
(a)Pattern distribution Q(j) and pattern entropy . . . 48
(b)Pattern transition matrix and pattern dynamical entropy . . . 49
Power spectra in space or time . . . 49

References 50

1 Introduction — Why Coupled Map Lattices?

Modelling and characterization of complex phenomena in spacetime is important in the study of turbulence in a general sense, not only in fluid dynamics but also in solid-state physics, optics, chemical reaction with diffusion, pattern formation problems, and possibly in biology. This kind of phenomena is called as "spatiotemporal chaos" [1], in an attempt to understand it on the basis of knowledge on dynamical systems theory, especially, chaos.

Several years ago, the author proposed a simple model with essential features of spatiotemporal chaos. In the present review, we first discuss the qualitative features of the model with some visualization, and then try to explore the universal scenario for pattern dynamics. We introduce some quantifiers to characterize the pattern dynamics, such as spatial-temporal power spectra, domain distribution as order parameters, Lyapunov spectra and mutual information flow and so on.

We briefly discuss some trials towards the construction of thermodynamics with the use of Perron-Frobenius operator and self-consistent approximation. Also we discuss the mean-field version of the present model briefly.

Some applications to physical, chemical and biological systems are also discussed, such as Benard convection, convection in liquid crystals, Taylor flow, open flow in fluid systems, chemical reaction with diffusion, some solid-state systems such as Josephson junction array, charge density wave, spin wave turbulence, spinodal decomposition, and possibly some biological networks [2].

The model we use here is a coupled map lattice (CML) [1,2,3,5]. It has been recently investigated extensively in various contexts [1-43].

A CML is a dynamical system with a discrete time, discrete space, and continuous state [1,2,3,5,6] see also, [9,10,12]). A modelling of physical phenomena by CML is based on the following steps:

Our strategy of studying dynamical phenomena in spatially extended systems by CML is based on the following steps:

(A) Take a (set of) field variable(s) on a lattice.

(B) Decompose the phenomena into independent units (e.g., convection, reaction, diffusion, and so on)

(C) Replace each unit by the possible simplest parallel dynamics on a lattice: the dynamics consists of nonlinear transformation of the field variable on each lattice point and/or a coupling term among suitably chosen neighbors.

(D) Carry out each unit dynamics ("procedure") successively.

Let us take the simplest example, that is the local nonlinear process and diffusion, as can be seen in the reaction-diffusion system. As the independent units, we take local nonlinear process $x(i) \to x'(i) = f(x(i))$ and the discretized diffusion process $x'(i) \to (1-\epsilon)x'(i) + (\epsilon/2)[x'(i+1) + x'(i-1)]$. Combining these two procedures, our dynamics can be written as

$$x_{n+1}(i) = (1-\epsilon)f(x_n(i)) + \epsilon/2[f(x_n(i+1)) + f(x_n(i-1))] \qquad (1)$$

where n is a discrete time step and i is a lattice point ($i = 1, 2, \cdots, N$=system size)

[1] This term is often used incorrectly, that is for the low-dimensional chaos with some spatial structure. Here we use the term for the high-dimensional chaos whose dimension (effective degrees of freedom) diverges with a system size.

[2] This area of the field is rapidly growing recently and it is impossible to cover in a short review.

with a periodic boundary condition. Extensions to a higher dimensional lattice are straightforward which will be discussed in §3.

Here the mapping function $f(x)$ is chosen to be the logistic map

$$f(x) = 1 - ax^2, \tag{2}$$

since the map has already been investigated in detail. Features in the logistic map lattice, however, can be seen in a wide class of mappings and in other types of couplings, and are thought to be rather universal in a system with local chaos and diffusion. If we adopt a different class of mappings like circle map $f(x) = x + (K/2\pi)sin(2\pi x) + \Omega$, or a bistable map $f(x) = tanh(\beta x)$, different behaviors can be seen (soliton turbulence and pattern formation respectively).

In the model (1), the independent procedures in (B) are local transformation (eq.(2)) and the diffusion process, which are separated parallel procedures. The model consists of the sequential repetition of these two procedures. This argument leads to the following equivalent form with the above model:

$$y_{n+1}(i) = f((1-\epsilon)y_n(i) + \epsilon/2(y_n(i+1) + y_n(i-1))). \tag{3}$$

If we adopt different procedures, we can construct models for different types of dynamical behavior of spatially extended systems. Examples with a different type of coupling ("convective coupling") will be studied in §8. Other choices of nonlinear process for the construction of CML corresponding to the spinodal decomposition, excitable media, Josephson junction and so on are also discussed.

Let us compare the merits and demerits of our model with other models for spatially extended systems, in particular, partial differential equation (PDE) and cellular automata (CA)[44].

PDE vs. CML

A merit of PDE over CML is that it is easily related with physical phenomena[3], starting from macroscopic equations such as the Navier-Stokes. Reduced equations can be obtained with the use of some perturbative techniques (e.g., reductive perturbation method). Analytic methods developed since Fourier are available for PDE.

Merits of CML over PDE are that (i) straightforward application of dynamical systems theory, in particular, chaos (ii) straightforward connection with the studies in statistical mechanics on a lattice system and (iii) numerical efficiency which enables us a global search in the parameter space.

CA vs. CML

Since there is no inherent continuos parameter in CA, it is rather difficult to see a change of a state with a change of parameter. Applications of dynamical systems theory are difficult in CA. Another drawback in CA is that it cannot create information in the sense of Shannon [22]. In a finite lattice, information in CA is finite, of course, and there is no "creation of information" in the bit space. Another technical drawback in CA is that an aperiodic state exists only in a lattice of an infinite size. One has to discuss an asymptotic behavior as a system size gets large. However, it is not always

[3]This, however may be just a prejudice produced through long-term history.

easy to distinguish if the relevant behavior in an infinite system comes from a transient or a periodic attractor in a finite lattice [4].

In CML, notions developed in dynamical systems theory can be extended, while the straightforward application of notions in information science [45] is possible in CA.

As for the efficiency: In recent days, the use of "lattice gas automata" to fluid dynamics is becoming popular [46]. Numerical efficiency is stressed in this kind of approach in the term of "bit democracy", which means that each bit is used almost equally in the course of computation. It is thought that this method is very efficient if a special purpose machine is constructed. This is not necessarily true.

Indeed, there are two merits of CML over CA.

First, a field variable in CML is a quantity after a coarse graining. In CA, each cell corresponds to a microscopic variable. Thus we need a very large lattice size to have a realistic simulation. On the other hand, we can get a suitably statistical behavior within a small lattice system in CML. Statistical physics is science of coarse-graining, and it is obvious that a suitably coarse-grained model is in higher level description of the nature.

The second point is more technical. In the present computer with floating processors, hierarchical use of bits is quite fast, where bits are not used in an equal weight. On the other hand, in the architecture of digital computers, discreteness of time and space are not overcome. This leads to an efficiency of models with continuous state, discrete time and space [5].

2 Pattern Dynamics in a 1-dimensional Lattice

2.1 Global phase diagram

First we show a global phase diagram in our coupled logistic lattice, which is obtained by the simulation of (1) with random initial conditions. The meaning of each phase in the figure is explained in the course of the paper. Some examples of the space amplitude plots are shown in Fig.2, where patterns $x_n(i)$ from many time steps are overlayed. Also, examples of space-time diagrams are given in Fig. 3.

Let us briefly survey the characteristic property of each phase, with the use of spatial power spectra, and Lyapunov spectra.

Detailed account of a feature of each phase will be shown in the following sections.

Spatial power spectra

Spatial power spectra ($\Rightarrow$ Appendix) for each phase are given in Fig. 4. We note the following changes:

i) In the frozen random phase, the spectra decay slowly (roughly by $exp(-k)$). This comes from a random configuration of domains (Fig.4a).

ii)Few peaks grow at the pattern selection regime. The peak(s) are located at the wavenumber of selected patterns (Fig.4b).

[4]We may distinguish the two by growth rates of transients and period of attractors in a finite lattice. It depends on rules which of the period or transients grows faster with the system size [50].

[5]The purposes of the present paper are two-fold. One is to see the phenomenology of spatiotemporal chaos studied in CML, and the other is the application of CML to physical phenomena. If the reader is interested only in the latter aspect, (s)he can skip the details of §2 -7 and jump to §8.

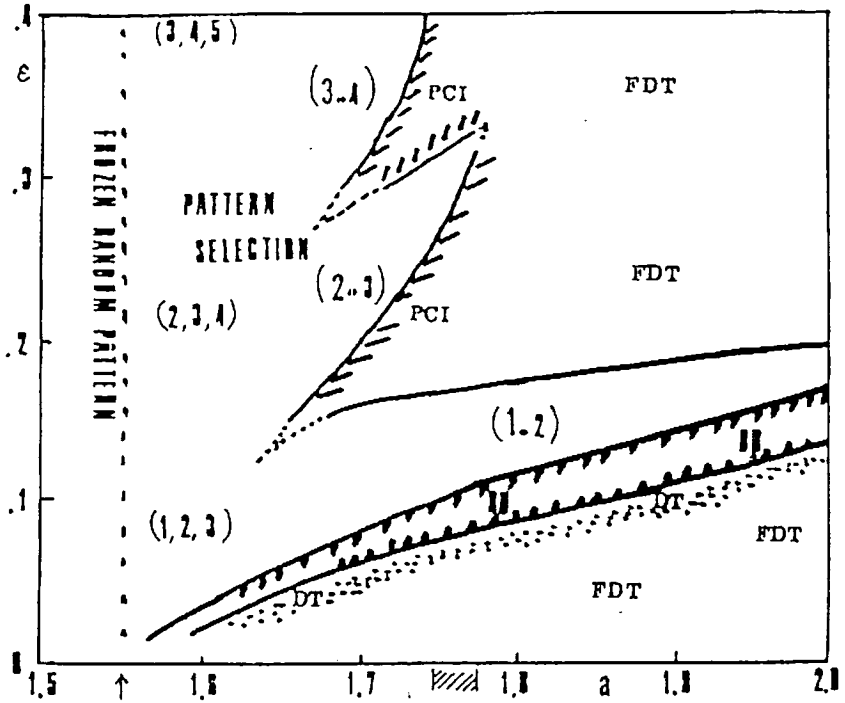

Fig.1: Phase diagram of the coupled logistic lattice (1): The phases are determined by the spatiotemporal patterns and the distribution function of pattern $Q(k)$ to be defined later. Simulation has been carried out for (1) with random initial configurations and N=100. The parameters are changed from a=1.5 to 2.0 by 0.01 and ϵ = 0.02 to 0.4 by 0.02. Here BD, DT, PCI, and FDT are the abbreviations of Brownian motion of Defect, Defect Turbulence, Pattern Comepetition Intermittency, and Fully Developed Turbulence, respectively, which are discussed in detail later. The numbers such as 1,2,3 represent the selected domain sizes. See text for details. The arrow at the bottom line shows the band merging point for the single logistic map, while the region with oblique lines correspond to the period-3 window in the logistic map. (Reproduced from Ref. [3])

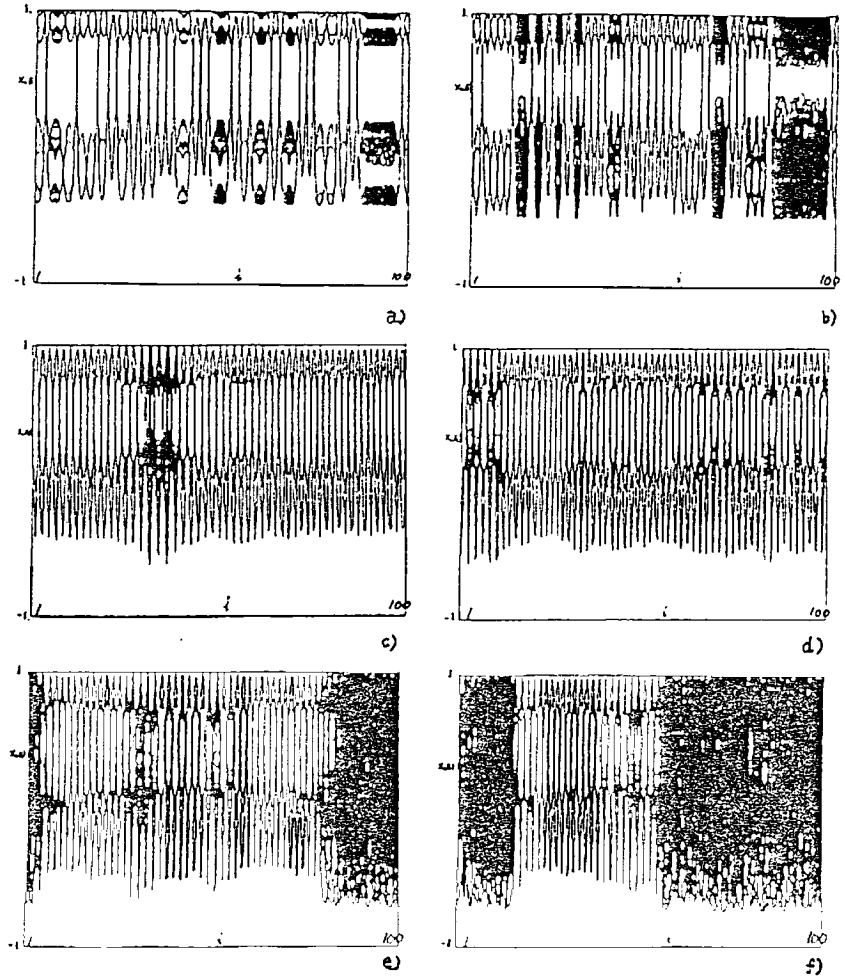

Fig.2: Space-amplitude plot for the coupled logistic lattice (1). Amplitudes $x_n(i)$'s are overlayed for 250 time steps after the 10000 transients. ϵ = 0.4, N=100, and random initial condition.
(a) a=1.42 (b) a=1.51 (c) a=1.65 (d) a=1.735 (e) a=1.737 (f) a=1.75

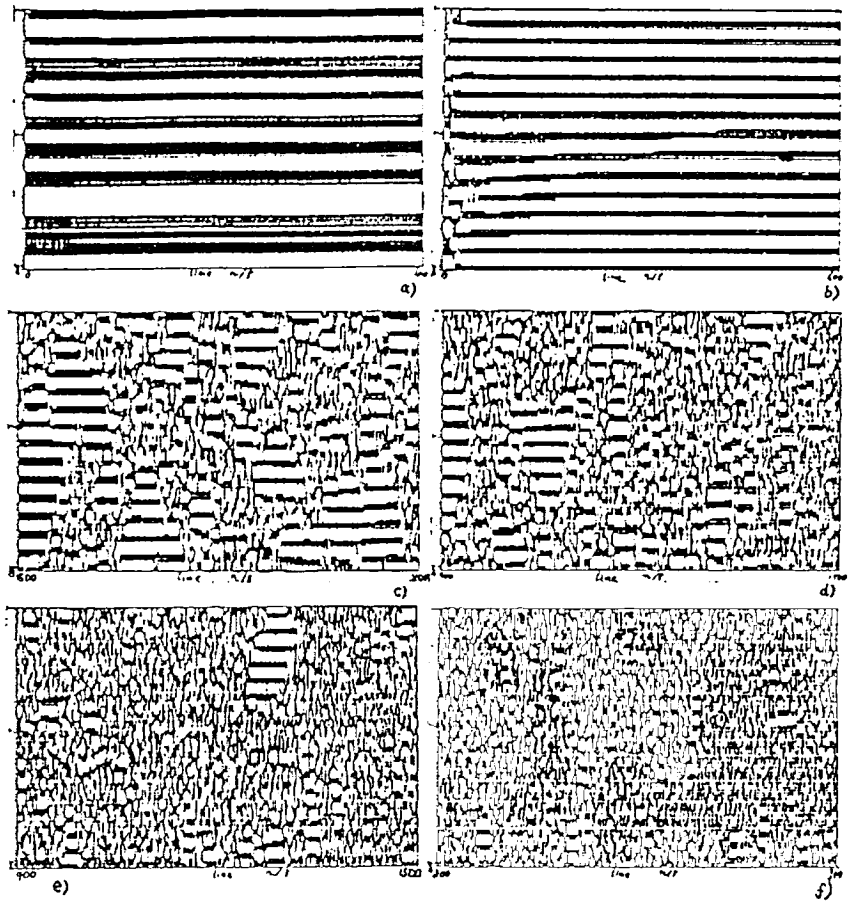

Fig.3: Space-time diagram for the coupled logistic lattice (1), with $\epsilon = 0.4$, N=100 and starting with a random initial condition. Every 8th step is plotted. If $x_n(i)$ is larger than x_*(unstable fixed point of the logistic map) , the corresponding space-time pixel is painted as black (if $x > x_1^* \equiv (\sqrt{1+7a}-1)/(2a)$ painted darker), while it is left blank otherwise.
(a) a=1.5 (b) a=1.68 (c) a=1.75 (d) a=1.77 (e) a=1.83 (f) a=1.88

iii) Coexistence of the sharp peak(s) and the broad band noise at $k \approx 0$ for the defect turbulence and the pattern competition intermittency. In the defect turbulence, the peak at $k = 1/2$ and the broad band noise around $k = 0$ coexist. The latter part increases as the nonlinearity is increased. In the intermittency case also, the burst brings about the broad band spectra at $k = 0$ for $S(k)$. The whole spectra are composed of the broad-band and the sharp peaks at the wavenumbers corresponding to the selected patterns. As the nonlinearity is increased, the portion of the broad band noise increases (see Fig.4c).

iv)Fully developed spectra: As the nonlinearity a is increased further, sharp peaks disappear completely (see Fig.4d). The spatial spectra decay monotonically as k. They are roughly fitted by the form of $exp(-const. \times k^2)$. This Gaussian form arises from the diffusion nature of our model.

Temporal power spectra

Temporal power spectra (⇒ Appendix) are useful to characterize the temporal behavior of the system.

In the frozen random pattern, the peak at $\omega = 1/2$ is seen as is expected since a single logistic map exhibits the period-2 band motion for this parameter range. In the pattern selection regime, the above peak (and some other peaks in some cases) are observed, which is due to the regular motion by the pattern selection mechanism, to be discussed in §2.3. At some parameters, the motion is quasiperiodic in time and the peaks are located at $n(1/2) + m\omega$ (n, m are integers, and ω is an irrational number). In the fully developed turbulence, the peaks disappear and are replaced by some Lorentzian band noise around it and around $\omega \approx 0$.

Lyapunov analysis

The stepwise structure is seen in the Lyapunov spectra(⇒ Appendix) in the frozen random phase, which reflects upon the degeneracy by the existence of separated domains (see Fig.5a)b). Localized chaotic motion exists only in large domains, which gives positive Lyapunov exponents. The number of the positive exponents is proportional to the number of such domains. Here KS entropy (⇒) increases with a (Fig.6).

The values and the number of positive Lyapunov exponents decrease by the pattern selection, as is seen in Fig.5 c)d). Also, we can see that the KS entropy in Fig.6 shows a sudden decrease at $a \approx 1.56$. These show the suppression of chaos by the pattern selection clearly. In the pattern selection regime, still the stepwise structure is seen since there are degeneracies due to the existence of domains of the same size.

In the intermittency region, there are some positive exponents which are not very close to zero. The stepwise structure disappears here since the burst destroys the separated domain structure. The spectra as a whole take a rather smooth shape.

In the fully developed turbulence (Fig.5 e)f)), spectra are smooth in form. At the onset of spatiotemporal chaos, the spectra shape are close to be linear (Fig.5 e) ($\lambda_i = const. - ri$). As the nonlinearity is increased the shape increases its concavity,indicating

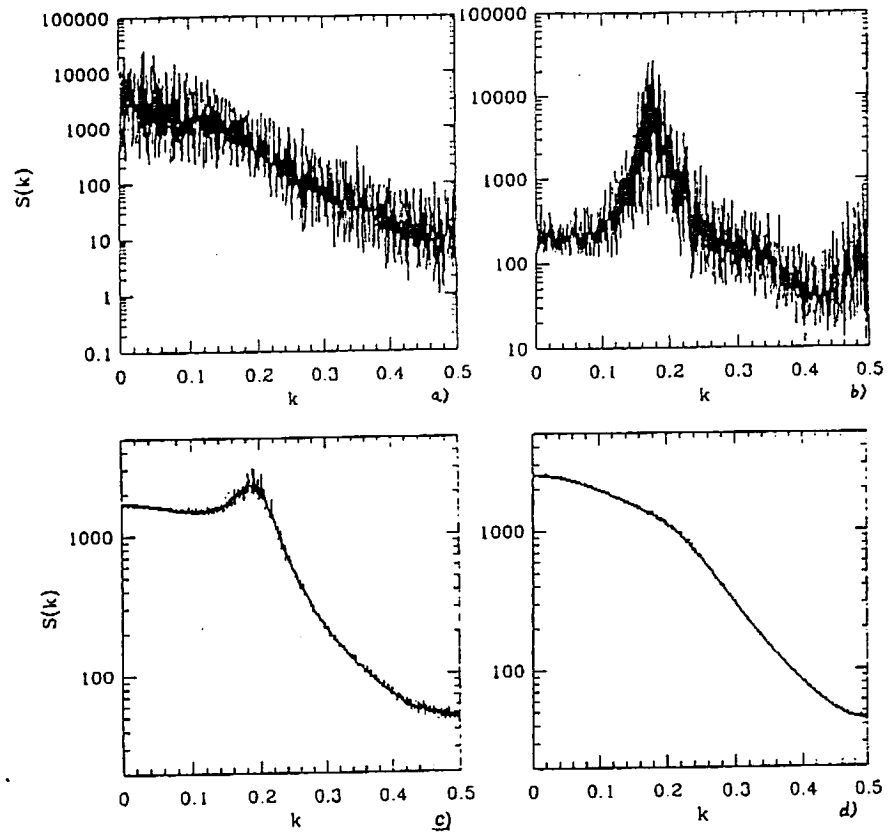

Fig.4: Semi-log plot of spatial power spectra S(k) for the model (1), with $\epsilon = .3$, N=4096, and starting with a random initial condition. Calculated from 10000 time step averages after discarding 10000 transients.
(a) a=1.53 (b) a=1.69 (c) a=1.78 (d) a=1.93

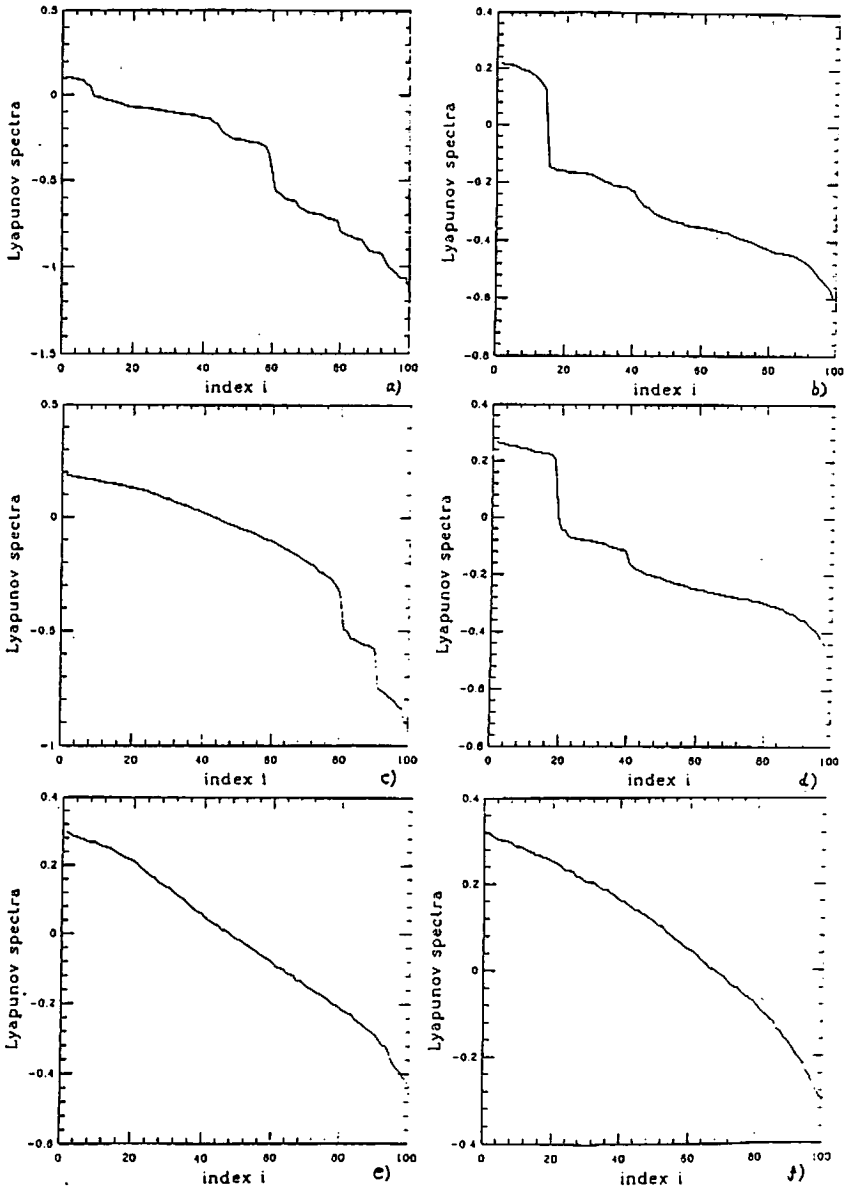

Fig.5: Lyapunov spectra of our model with $\epsilon = .2$, starting with a random initial condition. The calculation was carried out through the products of Jacobi matrices of the time steps 2000 to 5000. N=100.
(a) a=1.45 (b) a=1.55 (c) a=1.65 (d) a=1.7 (e) a=1.75 (f) a=1.85

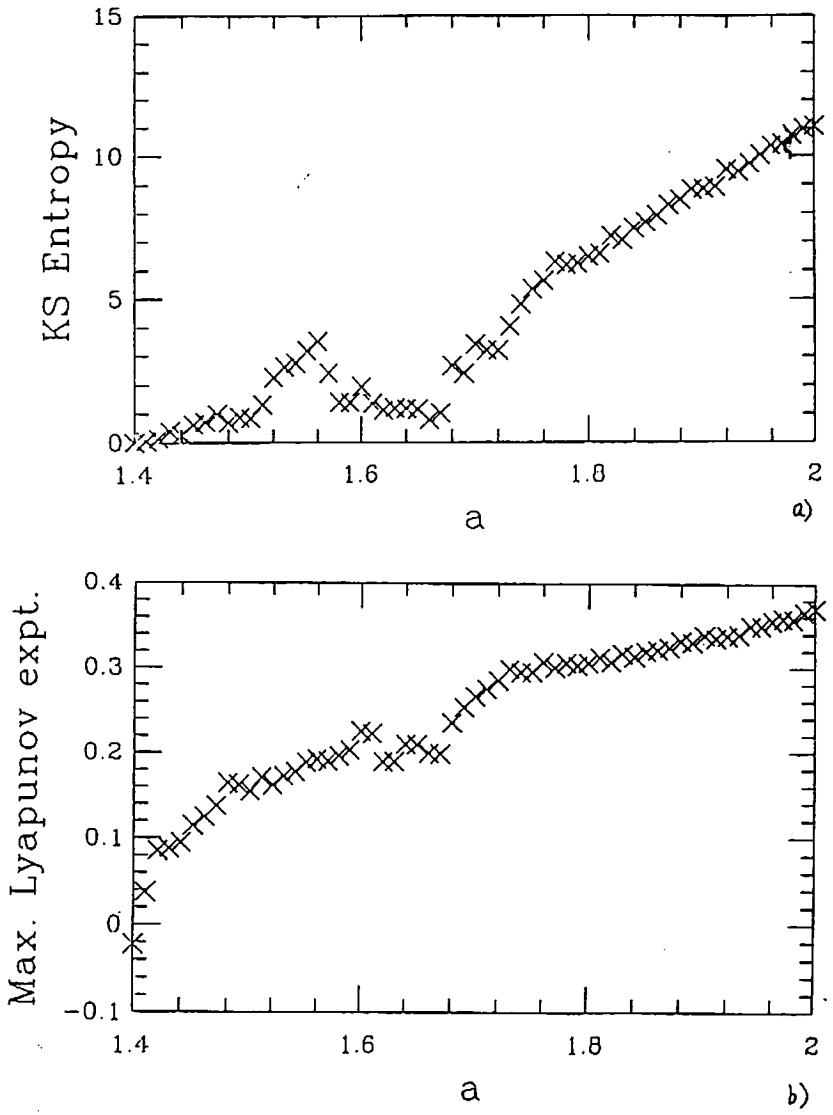

Fig.6: KS entropy (a) and maximal Lyapunov exponent (b) as a function of a, calculated from the Lyapunov spectra in the same way as in Fig.5. $\epsilon = .2$, N=64. To get the KS entropy density divide the values in the figure by $N = 64$.

the approach to independent chaotic motions of elements.

In the following sections we discuss the nature of each phase in a little more detail.

2.2 Frozen random pattern

CML (1) exhibits the period-doubling of kinks with the increase of the nonlinearity a. By the doublings, domains of various sizes are formed. After some numbers of doublings, the system exhibits a chaotic behavior at large domains. The domain boundary does not move in space (Fig. 2a)b), Fig.3a)).

As is seen in the phase diagram (Fig.1), the single logistic map here is in the parameter region for the band splitting with a period-two-band motion. The domain separation is assured by this band splitting.

In a large domain, the motion is quite chaotic, while it is almost period-8 at smaller domains, period-4, for much smaller domains, and period-2 for the smallest ones. We note that the motion of the lattice point differs in space ("spatial bifurcation"), although the dynamics itself does not include any inhomogeneity in space.

Distribution of domain sizes can differ by initial conditions. We can choose initial conditions so that attractors have an arbitrarily large domain. Thus we expect that the number of attractors increases exponentially to the system size.

2.3 Pattern selection and suppression of chaos

As the nonlinearity is increased further, larger domains start to be unstable and split into smaller domains. Initial conditions are no longer preserved (Fig.3b). Through the transient process, domains of few special sizes are selected. As the nonlinearity is increased, the number of possible patterns decreases and at the medium nonlinearity, only $1 \sim 3$ patterns are selected (Fig.2c)d)e)).

After the selection, the pattern of domains is frozen and does not move in space. Selected sizes of domains are such that the dynamics in the domains is less chaotic, that is, the motion with shorter periods. In the frozen random pattern, chaos is suppressed only in domains of small sizes. Here, only such small domains are selected.

A precise definition which distinguishes the frozen random state from the pattern selection is given by the following: In the frozen random phase ($a < a_p \approx 1.54$), there appears an arbitrary large domain if the system size goes infinity, while there exists a critical size ℓ_c, such that a domain of the size larger than ℓ_c cannot exist. Decrease of the variety of domain size is clearly seen in the decrease of static pattern entropy ($\Rightarrow$ Appendix).

As has been discussed in the temporal power spectra, the motion here is quasiperiodic or slightly chaotic, which is clearly seen in the calculation of Lyapunov exponents. In fact the maximal Lyapunov exponent is close to be zero or very small. Suppression of chaos by the pattern selection is seen in the decrease of KS entropy ($\Rightarrow$Appendix) at $a > a_p$ [3].

The diffusion term has a tendency to produce the homogeneity in space, while the chaotic motion makes the system inhomogeneous due to the sensitive dependence on initial conditions. These two tendencies conflict with each other. The conflict leads to the splitting of a larger domain. (One may regard this as the splitting by the "chaos pressure".) On the other hand, there is no conflict if the domains are selected in which

chaos is suppressed. In this sense, we may term the present phase as " pattern selection through transient chaos and diffusion". Domains with larger positive exponents is easily collapsed by the boundary effect. This picture leads to the conjecture that *a pattern with smaller Lyapunov exponents is selected*. We have calculated Lyapunov exponents for various domain sizes by taking a small lattice size (2-10). Numerical results show that Lyapunov exponents are smaller (sometimes negative) in the selected domain sizes.

2.4 Selection of zigzag pattern and chaotic diffusion of defects

The simplest example of pattern selection is the selection of a zigzag pattern (domain size =1, i.e., $k = 1/2$). The zigzag pattern is easily characterized by the condition;

$$(x_n(i+1) - x_n(i))(x_n(i) - x_n(i-1)) < 0 \qquad (4)$$

or the condition $(x_n(i+1) - x*)(x_n(i) - x*) < 0$ with $x* = (\sqrt{1+4a} - 1)/(2a)$, an unstable fixed point of the logistic map $f(x)$.

As time goes to infinity, a single domain of zigzag pattern covers the whole space. In the transient time regime, we have seen defects as a domain boundary between two zigzag patterns with different phases of oscillations. The defect is localized in space and moves around. The motion of defects is chaotic in time, as is checked by positive Lyapunov exponents ($\Rightarrow$ Appendix).

An example of space amplitude plot for a single defect state is shown in Fig. 7, while an example of space-time diagram is shown in Fig. 8a). Defects pair-annihilate and a domain size of a connected zigzag region increases with time. The system finally settles down to the completely zigzag state if the system size is even ($Q(1) = 1, Q(j) = 0$ for $j > 1$), while only a single defect moves around the space if $N = odd$.

Diffusion coefficient of defects

The locus of the defect looks like the Brownian motion. We note that the diffusion process here takes place *not* in the phase space (as is often discussed in the study of chaos), but in the real space [53]. Here, it is not evident that the motion is really Brownian motion, since our system is deterministic. Let us check the property of the motion of defect in a little more detail.

By the pair-annihilation, the number of defects decreases as $n^{-1/2}$, for a large time step n, if we start from arbitrary chosen initial conditions. This decay is consistent with the Brownian motion picture of defects.

A way to see the motion of a single defect is to take a system with an odd number of size so that a single defect always exists. The position of defect I_n is calculated through the condition (4). The numerical data are well fitted by the following expression

$$< (I_n - I_0)^2 >= 2Dn, \qquad (5)$$

from which the diffusion coefficient D is calculated. Here the bracket $< ... >$ represents an ensemble average for a set of initial conditions.

The diffusion of a kink is observed in a cellular automaton problem [53], where the randomness comes from an initial random condition. The important difference here is that the randomness is created by the defect itself.

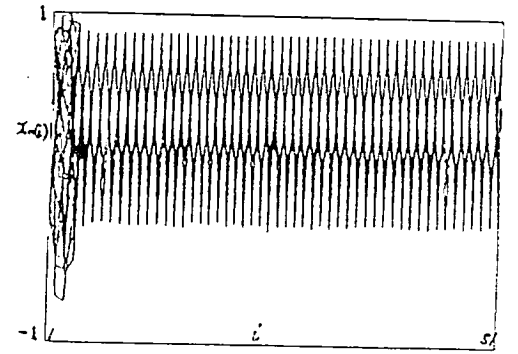

Fig.7: Space-amplitude plot for the coupled logistic lattice (1). Amplitudes $x_n(i)$'s are overlayed for 50 time steps after 1000 transients, starting from a random initial condition. N=51, $a = 1.83, \epsilon = .1$

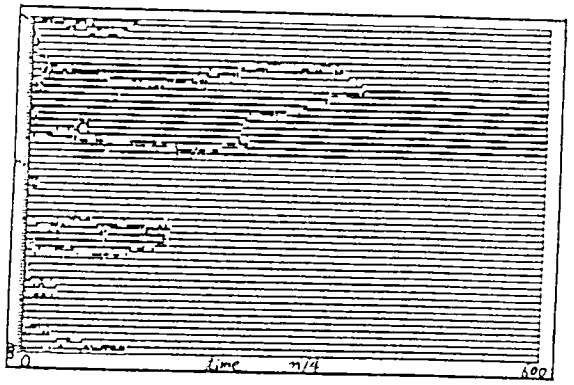

a)

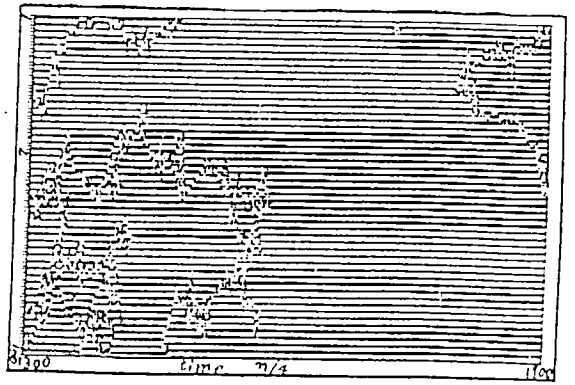

b)

Fig.8: Space-time diagram for the coupled logistic lattice (1), with $\epsilon = 0.1$, N=100 and starting with a random initial condition. Every 16th step is plotted. See Fig.3 for the way of digitization. (a) a=1.79 (b) a=1.885

The diffusion coefficient D is calculated as a function of a. It increases with a ($log(D)$ is roughly proportional to a).

To see if the defect is really chaotic, we calculate Lyapunov spectra for systems with a single defect and without any defects. If there is a defect, Lyapunov spectra have large positive parts, which are not seen in the spectra for a system without a defect. Kolmogorov-Sinai(KS) entropy of a defect is estimated by the sum of these positive parts. A logarithm of KS entropy increases linearly with a. Furthermore, the increase rate of a logarithm of the KS entropy and the diffusion coefficient agree if the zigzag region exhibits the chaotic motion.

KS entropy gives the rate of memory in the phase space. If the diffusion is triggered by the chaotic motion of a defect, the present Brownian motion can roughly be represented by a "coin tossing" per some time steps which are inversely proportional to the KS entropy. If this picture is valid, the KS entropy and the diffusion coefficient are proportional, which are consistent with our data in the chaotic regime.

2.5 Spatiotemporal intermittency transition: Defect turbulence and pattern competition intermittency

The selected pattern collapses at a critical parameter $a = a_c(\epsilon)$. Such a collapse of pattern occurs intermittently in space and time.

(I)Defect turbulence

At the region of $a \gtrapprox a_c$, the spontaneous collapse of zigzag pattern hardly occurs and the defect picture is still valid. At these parameter regions, the dynamics is governed by the pair-creation of defects, their Brownian motion, and collisions of defects, which may cause the pair- annihilation or creation of defects, or complicated transient patterns. The collision mechanism is quite similar to the "soliton turbulence" observed in coupled circle map lattices [11,5] and some cellular automata [50,52]. An example of space-time diagram is shown in Fig. 8b), where a pair-creation is clearly seen.

The phenomenon here can be understood as the crisis in a high-dimensional space (for crisis, see [54,55];see also [56]). The simplest way to see the relation with the crisis is the use of two-coupled logistic map ($N = 2$) [51]. If we plot the 2-dimensional attractor by $(x(1), x(2))$, the plot exhibits sudden broadening from two separated regions to a single connected region, at $a = a'$ which is slightly larger than a_c. As the size of our system N is increased, the onset parameter for the collapse of zigzag pattern decreases from a' to a_c. The reason for the suppression of the onset is that the gate for the crisis is increased as the size, since possible configurations of deviations from the zigzag structure are enriched. In other words, the discrepancy between a_c and a' arises from spatially chaotic modulations of the zigzag pattern.

(II)Selective flicker noise

A characteristic dynamical feature in the defect turbulence lies in its long-time correlation. To study this feature, we use the dynamical form factor (spatiotemporal power spectra (⇒Appendix).

In the parameter region of the defect turbulence, our system exhibits the following flicker noise for the modes with $k \approx 1/2$. In Fig.9, $P(k,\omega)$'s are plotted for k =0, 2/8, 3/8, and 1/2. As k approaches 1/2, low-frequency parts grow and $P(k,\omega) = \omega^{-\alpha}$ is

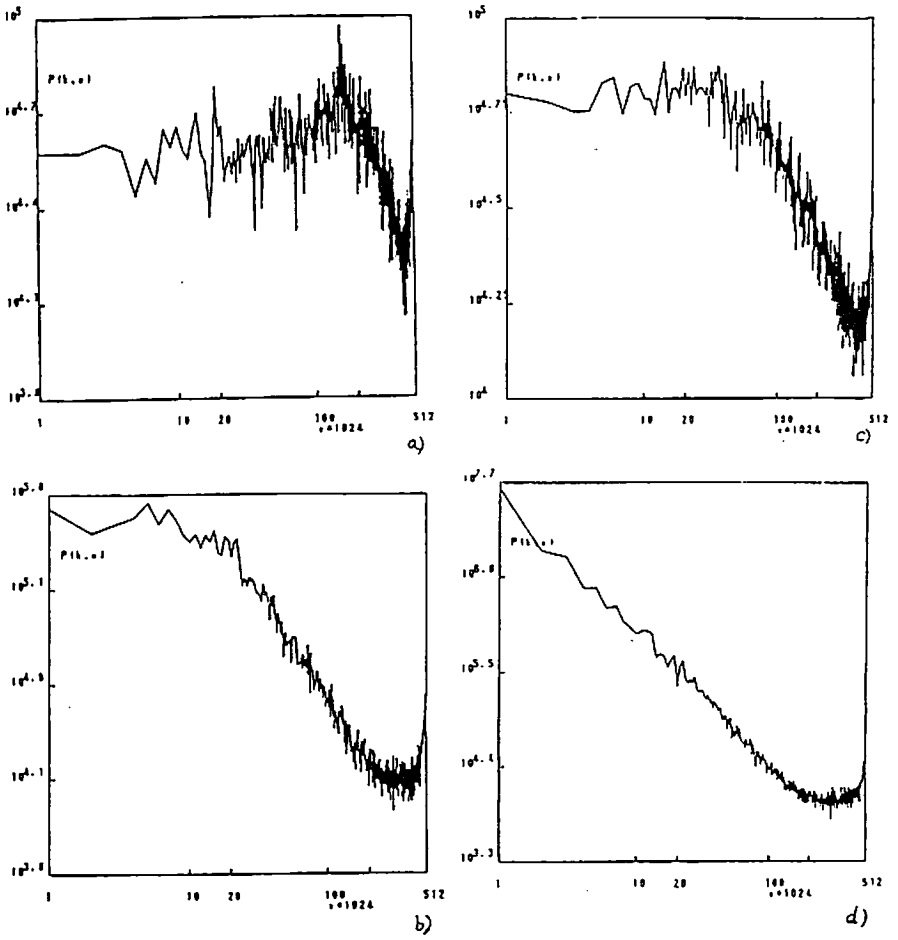

Fig.9: Log-log plot of space-time power spectra $P(k,\omega)$ as a function of ω for a=1.89, ϵ = 0.1: (a)k=0, (b)k=2/8, (c)k=3/8 (d)k=4/8. These power spectra are calculated from the data of $x_{2n}(i)$ for 512×2 time steps, after 10000 steps of transients, and from 50 sequential samplings, starting from a random initial condition (reproduced from [3]).

clearly seen for $k = k_1 (= 1/2)$. Note that the flicker noise is selectively observed only for the modes $k \approx 1/2$.

At the onset of the collapse of zigzag pattern ($a = 1.88$), α is close to 2, which means that the relaxation time diverges. As the nonlinearity parameter a is increased, the exponent α decreases from 2. The $\omega^{-\alpha}$ behavior is observed selectively for $k \approx 1/2$ at $a_c \approx 1.88 < a < 1.92 \approx a'$. Collapse of the zigzag pattern occurs more frequently for larger a, which leads to a faster decay of the correlation function (and small α).

The reason for this flicker-like noise is that the zigzag mode exists with a long range correlation, and it is destroyed only through a long-ranged effect as is seen in the above explanation by the high-dimensional crisis in the region of $a < a'$. Thus the dynamics of the mode of wavenumber 1/2 includes the motion of a very long time scale. On the other hand, the mode with $k \approx 0$ corresponds to the chaotic motion of defects, which has a short-time memory.

A reason for this critical behavior in a wide parameter regime may be attributed to the finiteness of system size. If we follow the common-sense of phase transitions, it is expected that a singular behavior is seen just at a critical point. The above power-law-type behavior in a large parameter space in a finite system, however, may be relevant in experiments, since most "large" nonequilibrium experimental systems (e.g., Benard convection, liquid crystal convection) contain $10^2 \sim 10^3$ effective degrees (e.g., number of rolls) which are much smaller than the Avogadro number.

Also, it is interesting to note that the critical behavior is easily observed in *temporal domains*, not in spatial domains (like correlation length).

As the wavenumber is decreased from $k = 1/2$, the power decreases gradually. As it goes much smaller, the plateau at $\omega = 0$ appears and the spectra approach the Lorentzian form.

The flicker-like noise has been observed in a low-dimensional dynamical system at the onset of chaos through the intermittency [57,58]. The flicker-like noise here should be noted for its selectivity to the wavenumber.

(III)Quantitative analysis of pattern dynamics

Pattern distribution function $Q(k)$'s ($\Rightarrow$ Appendix) are useful as order parameter(s) to distinguish the different phases observed in our model.

In the frozen random pattern, $Q(k) \neq 0$ for various k's. Furthermore, the distribution can depend on a choice of initial conditions. In the pattern selection regime, $Q(1)$ and $Q(2)$ get larger and ratios for larger domains are suppressed ($a > 1.58$). At $a > 1.64$ $Q(k) = 0$ for $k \neq 1, 2$. In these regions, the dependence of the distribution on initial conditions is very small if we restrict ourselves to random initial conditions and take a large N (say, > 100). In particular, the selection of $k = 1$ and 2 at $a > 1.64$ is not affected by the change of initial conditions. In the zigzag pattern selection phase, $Q(1) = 1$ and $Q(k) = 0$ for $k \neq 1$.

At $a > a_c$, the zigzag pattern collapses spontaneously. Thus $Q(k)$ $(k \neq 1)$ does not vanish. The value $(1 - Q(1))$ gives a measure of the destructed pattern.

Critical phenomena of the collapse of patterns are investigated through the disorder parameter $1 - Q(1)$. Near $a \approx a_c$, the data are fitted roughly by

$$1 - Q(1) \approx (a - a_c)^{\beta}, \tag{6}$$

with $\beta \approx 1.0$. These critical phenomena are explained as the crisis in a high- dimen-

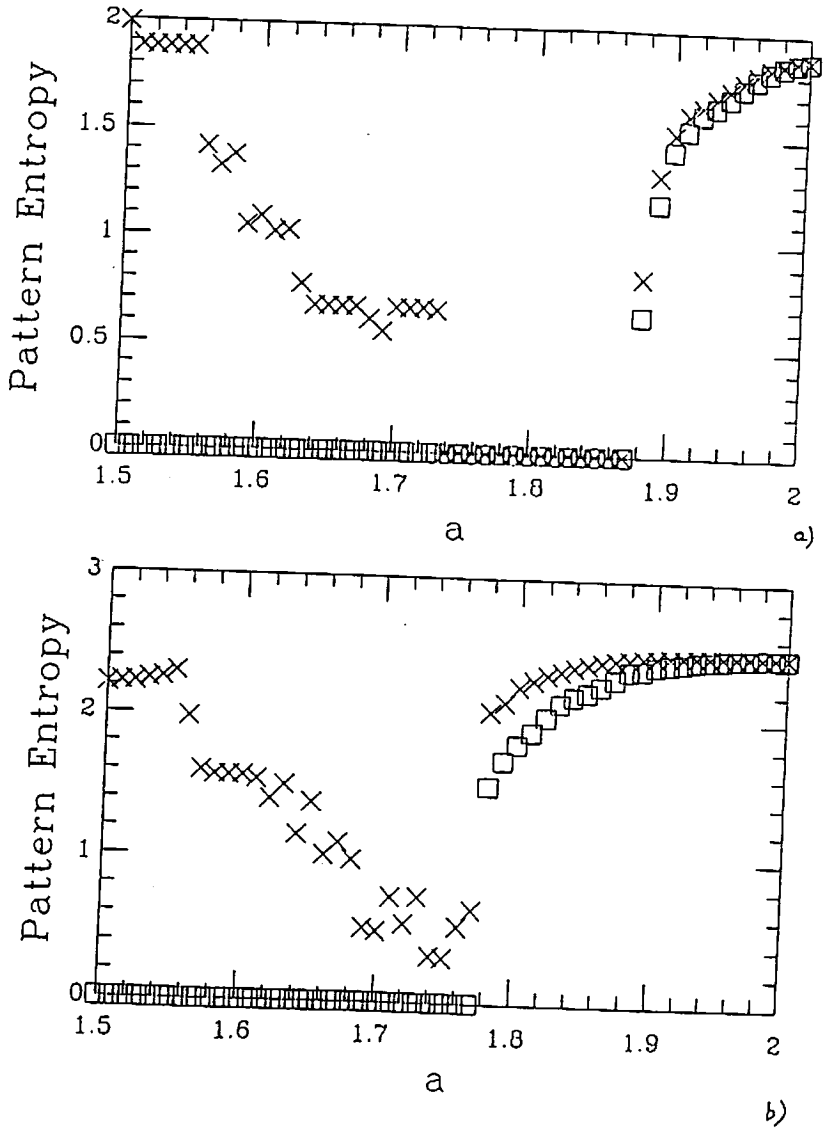

Fig.10 Pattern (static) entropy(×) and pattern dynamical entropy (□) for our model with N=128, calculated from the average for 30000 time steps after 10000 transients. (a) $\epsilon = .1$ (b) $\epsilon = .3$ (essentially reproduced from [3])

sional dynamical system in the terminology of dynamical systems. For the exponents in the crisis in low dimensional dynamical systems, see [55], where the exponents are related with the eigenvalues of saddles.

A single quantity to characterize the pattern complexity is an entropy(⇒Appendix). The change of static pattern entropy is shown in Fig.10. The entropy is large in the frozen random pattern, and decreases rapidly by the pattern selection to the zigzag state. By the pattern collapse it increases with

$$S_p \propto (a - a_c)^{\beta'}. \tag{7}$$

The exponent β' coincides with β within a numerical error as is expected, since $Q(k)$'s for $k > 1$ contributes to the increase of entropy.

Dynamical aspects of patterns are characterized by the transition matrix of patterns or (more simply) by the pattern dynamical entropy(⇒Appendix). In the frozen pattern, there is no transition among patterns. Thus the pattern dynamical entropy vanishes, even if the static entropy is large. At the onset of defect turbulence, the entropy increases with the form

$$S_d \propto (a - a_c)^{\delta}, \tag{8}$$

with the exponent $\delta \approx \beta$. Since this exponent includes the dynamical aspect also, it is probable that $\delta \neq \beta$.

A difference between the static and dynamic entropies shows how the patterns are spatiotemporally complex in the sense of mutual information (⇒Appendix). The difference is large in the defect turbulence (transition regime).

In the defect turbulence region, the transition matrix may not be a good quantifier, since the temporal correlation has a long-time-tail and is not represented by a Markovian dynamics. The lifetime distribution of the zigzag pattern does not show an exponential decay but has a Pareto-Zipf form, that is,

$$W_1(n) = n^{-\psi}. \tag{9}$$

The life-time distributions for the other sizes of domains have a normal exponential form $W_k(n) = exp(-n/t_{lf}(k))$, where $t_{lf}(k)$ is the lifetime of the domain of size k.

The Pareto-Zipf form is typically observed in the dynamics with the flicker-like noise (see e.g., [57]). Since the power spectra can be written as the sum of the temporal Lorentzian form as

$$P(k,\omega) \sim \int dn W_j(n)/(\omega^2 + 1/n^2) \tag{10}$$

for the corresponding wavenumber k and the domain j, we can expect that the exponent ψ for domain size j and the low-frequency exponent α for the power spectra of the corresponding wavenumber ($k = 1/(2j)$) are related by

$$\psi + \alpha = 3. \tag{11}$$

From our numerical data, this equality is roughly satisfied [6].

[6] for a detailed account of a small discrepancy, see [3].

(IV)Pattern competition intermittency

If the coupling is larger, selected domain sizes are not unique, as can be seen in Fig. 3b). With the increase of nonlinearity, there appear intermittent bursts, which have a nonstationary nature (see Fig.2e),3d)). The burst arises from the mismatching of phases and has much larger structures than a chaotic defect.

The "pattern competition intermittency" here is characterized by the existence of more than one stable patterns and intermittent transition among patterns. Although each pattern remains to be stable by itself, the mismatch of phases of oscillations between domains creates some bursts, which move around in space-time and destroy the pattern. The long-range correlation in this phase is also remarkable.

The present intermittency has many aspects in common with the above defect turbulence. There are two different points: First, the number of selected patterns is more than one here. Secondly, the burst has much larger structures than a defect. This intermittency and defect turbulence belong to the spatiotemporal intermittency (STI), investigated extensively in recent years.

Spatiotemporal Intermittency

Here we briefly look back on STI. STI was first studied as the spatial extension [1,5] (see also [20]) of Pomeau-Manneville's intermittency [59]. The intermittency in the present model is related with the crisis in high dimensional systems (see also [10]). In the STI, local dynamics has topological chaos but a non-chaotic attractor. Through the coupling of the local dynamics, this unobservable topological chaos appears as the observable chaotic burst.

As for the phase transition problem, STI is quite close to the problem of directed percolation. (see also [60]). In some models, however, the critical exponents do not belong to the universality class of the directed percolation[20].

One interesting feature in the intermittency phase is the existence of long-lived transients. If a system size is small, the turbulent pattern can disappear after long transients, and the system finally hits a globally non-frustrated structure, and intermittent bursts disappear. Some of the spatiotemporal intermittency belong to a class of the transient turbulence, as is discussed in [23].

Selective Flicker Noise at the intermittency

In the pattern competition intermittency, we have again observed the selective flicker noise.

At $\epsilon = .3$ and $a = (1.72 \sim 1.76)$, for example, the dynamical form factor $P(k,\omega)$ near $k = 0$ and $k = 1/2$ obey the normal Lorentzian form, while the flicker-like noise is seen around $k = (1/6 \sim 1/3)$, which is fitted by $P(k,\omega) = \omega^{-\alpha}$. ($\alpha \sim (1.5 \sim 2.0)$). At these parameter regions, we have seen the pattern competition intermittency with the selection of domain sizes =2 and 3. The exponent α is ≈ 1.5, for $a = 1.73$.

Quantifiers for pattern dynamics

Pattern dynamical quantifiers show a similar critical behavior as in the defect turbulence.

In the frozen regime, there are various possible patterns which give a large pattern entropy and a vanishing dynamical entropy. As a is increased, the pattern selection process occurs and leads to the decrease of the pattern entropy.

In the intermittency region, the distribution $Q(k)$ consists of the domains of selected patterns (size=2 and 3 for $\epsilon = .3$) and the distribution function by the burst, which has the tail of $exp(-const. \times k)$. Through the collapse of pattern, we can see the critical behavior of the disorder parameter $(1 - \sum_p Q(p))$ (where the sum is over the possible selected patterns, e.g., $p = 2, 3$ for $\epsilon = .3$) and of the entropies, in a similar manner as in the defect turbulence.[7]

In the intermittency region, the lifetime distributions of domains of selected sizes (2 and 3 for $\epsilon = .3$) again shows the power-law. For example, $W_2(n)$ and $W_3(n)$ are fitted by $W(n) \propto n^{-\psi}$ with $\psi \approx 1.75$, for $a = 1.72$ and $\epsilon = .3$, while the lifetime distribution $W_4(n)$) obeys the usual exponential decay. Here again, the exponents ψ and α roughly obey the relation $\psi + \alpha = 3$.

2.6 Fully developed turbulence

As the nonlinearity is increased further, the ordered structure in the space-time diagram can hardly be observed (see Fig. 3e)f)). We call this state "fully developed turbulence" in our lattice system, since this state can be well approximated by the direct product state of local chaos with a rapid decay of spatial correlation. The state can be represented by smooth statistical and dynamical quantifiers. The change of $Q(k)$ with the nonlinearity a is smooth. Pattern distribution function obeys $Q(k) = exp(-const. \times k)$ for large k, which implies that the patterns are generated randomly. This means that the pattern dynamics is well approximated as a Markov process of 1-0 sequence. The difference between the dynamical and static entropies is small, indicating that the transition among patterns is no more restricted and occurs randomly. As for the conflict between the two tendencies (ordering by diffusion and inhomogenizaion by local chaos), the chaotic part exceeds in the ordering process in this phase.

The motion here is roughly approximated by the "heat bath" picture. Take a subsystem, and our dynamics in the subsystem is well approximated by the local deterministic chaos by the variables within the subsystem and the random perturbation from boundaries, which is created by the chaotic motion from other areas. This picture leads to the "self-consistent" Perron-Frobenius theory as is discussed in §6.

2.7 Summing Up...

The main results in §2 are briefly summarized in Table I.

We note that our transition sequence has similarity with the phases in gas, liquid, crystal, and glass. The fully developed turbulent phase can correspond to the gas, while the pattern selection is analogous with the ordered pattern in a crystal. In a frozen random phase, the randomness in a large domain or in a defect is frozen in space, which reminds us of the frozen randomness in the glass. As the nonlinearity is increased, the local chaos in our system is amplified ("temperature is increased"), which leads to the "melting" of frozen patterns successively.

[7] detailed quantitative studies are left for future.

Before closing the present section, we note the tongue structure of pattern selection in the phase diagram (Fig. 1). This kind of tongue-like structure of spatial locking structure is seen in a static pattern of spatially modulated systems (see e.g., [47,48]) and in the resonance structure in low dimensional dynamical systems (Arnold tongue; see e.g., [2]). The pattern selection in our model corresponds to the resonance structure in space. Our result shows that the spatial locking is also seen in the problem of the pattern selection in spatiotemporal chaos, if the selected pattern is fixed in space.

Table I. Features of phases characterized by quantifiers.

Quantifiers	Temporal power spectra	Spatial power spectra	Pattern Distribution $Q(k)$	Pattern Entropy S_p	Dynamical Entropy S_d	Lyapunov Spectra	KS Entorpy
Frozen Random Pattern	Peaks+ Broad Band Noise	$exp(-cst. \times k)$	$Q(k) \neq 0$ for many k's	Large (almost constant)	0	Small stepwise structure	Positive
Pattern Selection	Peaks+ Broad Band Noise	Few peaks (+ Noise)	few $Q(k)$'s $\neq 0$ $Q(\ell) = 0$ for $\ell > \ell_c$	Small $\searrow$	0	Large stepwise structure	Small $\searrow$ (or 0)
(Intermittency)	Broad peaks+ Noise	Broad peaks+ Noise	few peaks and $exp(-cst. \times k)$	$(a - a_c)^{\beta'}$	$(a - a_c)^{\delta}$	positive parts grow	start to $\nearrow$
Fully Developed Turbulence	Broad Band Noise	$exp(-cst. \times k^2)$	$Q(k) \propto exp(-cst. \times k)$	Large $\nearrow$	Large $S_d \approx S_p$	Smooth form	Large $\nearrow$

3 Pattern Dynamics in a 2-dimensional Lattice

Extension of our diffusively coupled map lattice to a two-dimensional space is quite straightforward. Here we consider the simplest case, i.e., the nearest-neighbor coupling on a square lattice (see also [16]). The model is given by

$$x_{n+1}(i,j) = (1-\epsilon) f(x_n(i,j)) +$$

$$\epsilon/4[f(x_n(i+1,j)) + f(x_n(i-1,j)) + f(x_n(i,j+1)) + f(x_n(i,j-1))] \qquad (12)$$

where n is a discrete time step and i, j denotes a 2-dimensional lattice point ($i, j = 1, 2, \cdots, N$=system size) with a periodic boundary condition. Here the mapping function $f(x)$ is again chosen to be the logistic map $f(x) = 1 - ax^2$.

Examples of snapshots are shown in Fig. 11.

For small ϵ, we have again observed the transition sequence from (i) frozen random state to (ii) pattern selection and to (iii) fully developed turbulence via spatiotemporal intermittency.

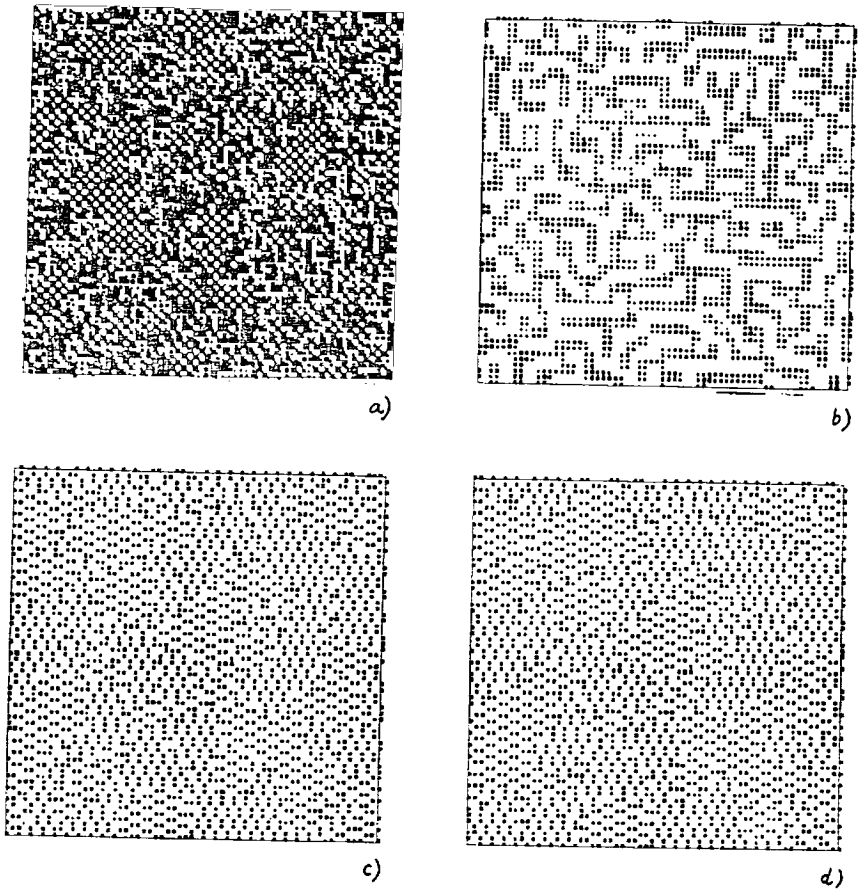

Fig.11: Snapshot pattern for the 2-dimensional logistic lattice. On a lattice point (i,j), a square with a length proportional to $(x_n(i,j)-0.2)$ is painted if $x_n(i,j) > .2$. Otherwise it is left blank. Size = 64x64.
(a)a=1.903, $\epsilon = .1$, at time step 6000
(b)a=1.8, $\epsilon = .35$, at time step 5000
(c)a=1.94, $\epsilon = .2$, at time step 15000 , (d) time step 40000.

3.1 Checkerboard pattern selection, chaotic string, and spatiotemporal intermittency

For $\epsilon = .1$, a frozen random pattern is observed for $a < 1.75$ (Fig. 6a). A checkerboard pattern is selected for $1.75 \leq a \leq 1.9$ (see Fig. 12) . After some transients, a single checkerboard pattern covers the whole space if the size is even. The selection process is regarded as the pattern formation, since two antiphased checkerboard domains are separated by a string, which moves chaotically in time and moves around space, and disappears by the collisions.

The zigzag pattern formation (Fig.12) is quite similar to the process seen in the ordering process of magnetic systems, or of simulations in the kinetic Ising model or time-dependent Ginzburg-Landau equation (see also §8). We can see the pattern formation process by the Brownian motion of a chaotic string. Here we call the motion as Brownian, since the motion there obeys the normal diffusive behavior triggered by a random walk, as is seen in the Brownian motion of defects in §2. The chaotic motion of a string is again quantitatively checked by Lyapunov exponents. In the same manner as in the Brownian motion of defects, we can estimate the KS entropy of a chaotic string. In fact, we have (additional) positive Lyapunov exponents in the presence of a string, which cannot be seen in the complete checker-board pattern.

Question: Does the chaotic motion at the domain boundary give novel features in the pattern formation? Does it belong to the same universality class as the kinetic Ising model?

At $a = a_c \approx 1.901$, the checkerboard pattern collapses spontaneously. Defects are created spontaneously from the checkerboard pattern. For $a \approx 1.901$, these defects are not percolated. As a is increased further, they propagate and interact with each other. The interaction causes the spatiotemporal intermittency. The spatiotemporal pattern there is understood as the intermittent transition between checkerboards and random patterns (see Fig. 11a) for a snapshot).

The lifetime of checkerboard pattern has a power-law distribution near $a \approx a_c$, which leads to the selective-flicker-like noise again. In fact, we have calculated the dynamical form factor $P(k_x, k_y, \omega)$, a power of the Fourier transform in space and time. As in the 1-d case, it shows the selective flicker noise for the wavenumber of the checkerboard pattern, i.e.,

$$P(k_x = 1/2, k_y = 1/2, \omega) = \omega^{-\alpha} \tag{13}$$

($\alpha \approx 1.9$) while neither the spectrum $P(k_x = 1/2, k_y \approx 0, \omega)$ nor $P(k_x \approx 0, k_y \approx, \omega)$ does show the divergence of low-frequency parts (see Fig. 13 a)b)c)).

Recently Nasuno, Sano, and Sawada [62] have performed a beautiful experiment on the collapse of a grid pattern in the electric convection of liquid crystal. They found the intermittent collapse of the grid pattern and the selective flicker noise for the wavenumber for the grid pattern (with $\alpha \approx 1.9$).

3.2 Selection of larger patterns

2x1 pattern selection

If the coupling ϵ is increased, we have seen the pattern selection with larger wavelengths. If $\epsilon \approx .2$, the selected pattern is a 2x1 unit (see Fig. 11c)d)). In the selection of 2x1 unit, the transient time necessary for the pattern formation is much longer than

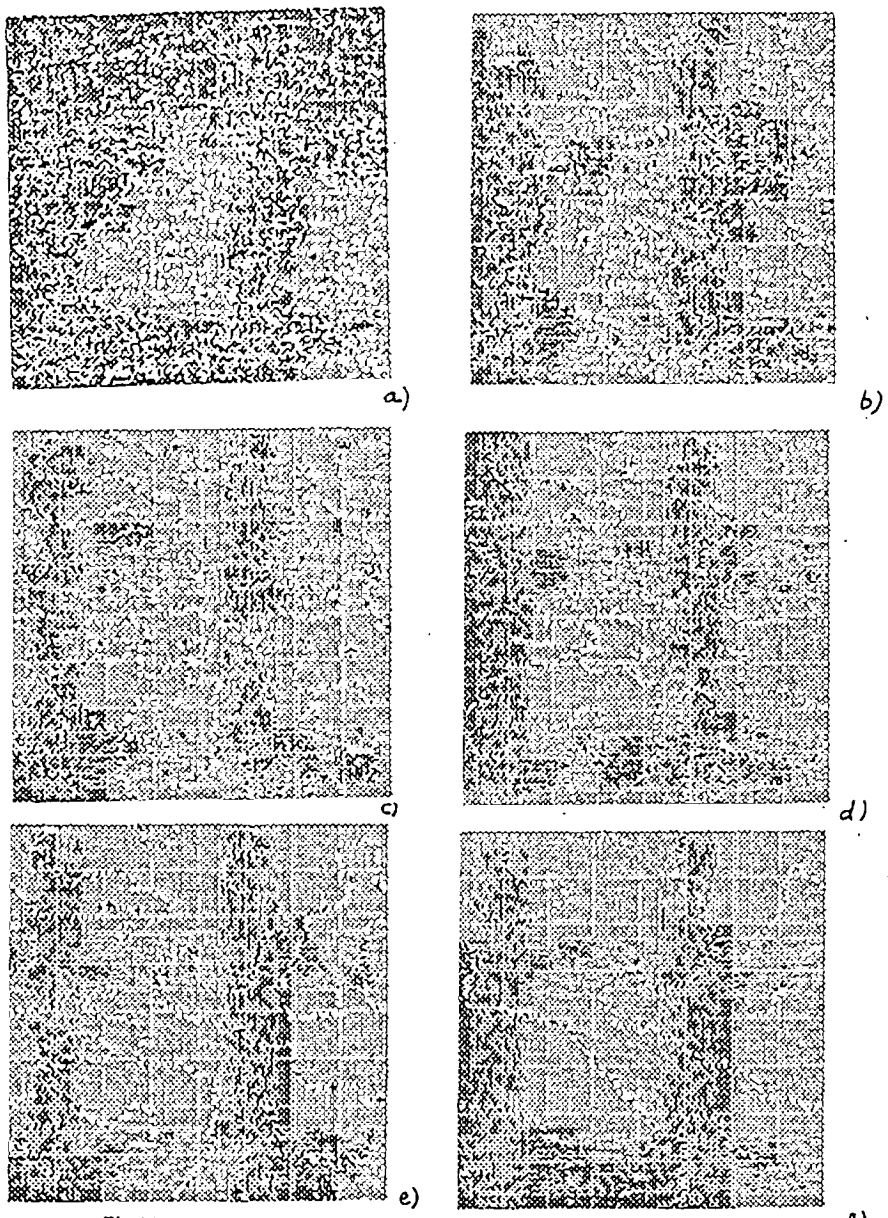

Fig.12: Brownian motion of chaotic string: Snapshot of the 2-dimensional logistic lattice. lattice size=128x128: a=1.8, $\epsilon = .1$
a) time step = 64 b) 192 c) 320 d) 480 e) 640 f) 1952

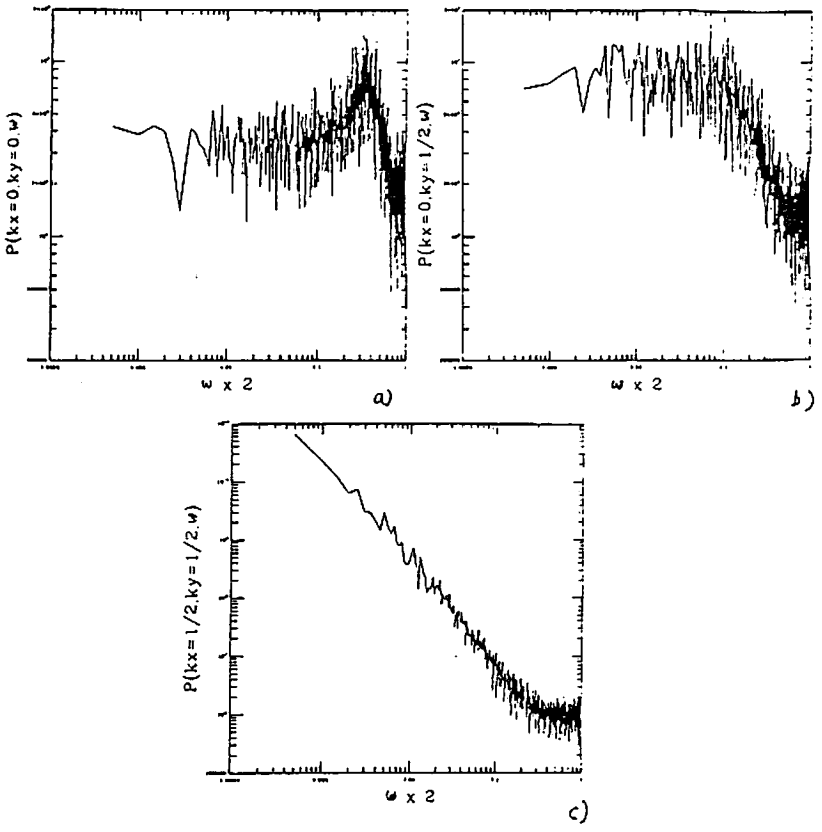

Fig.13: Log-log plot of $P(k_x, k_y, \omega)$ as a function of ω. a=1.904, $\epsilon = .1$. The spectrum is calculated from 10 sequential samples of 4096 steps after 2000 transients for the logistic lattice with the size of 64x64. (a) $k_x = k_y = 0$ (b)$k_x = 0, k_y = 1/2$ (c) $k_x = k_y = 1/2$.

that for a checkerboard pattern. This formation process is very slow because it is the competition process among 4 types of attractors (two types of phases of oscillations, and horizontal and perpendicular roll structures). This kind of pattern was first noted in a phase transition in a 2-dimensional stochastic cellular automaton [61].

Here again, chaos is suppressed by the pattern selection process, which is quantitatively characterized by the decrease of KS entropy.

As the nonlinearity is increased, a collapse of the pattern by the spatiotemporal intermittency again occurs. The existence of 4-fold degeneracy strongly suggests the first order transition, which is true in the 2-dimensional stochastic cellular automaton [61].

If the coupling ϵ is between .1 and .2 (e.g., .15), the competition between the checkerboard and 2x1 is seen, which leads to the intermittent collapse of the two patterns (pattern competition intermittency), or leads to a chaotic string with 2x1 structure in the zigzag domain. These are again similar to the observation in a 1-d lattice. In the experiment by Nasuno et al., these behaviors are again found [62].

labyrinth

We have not yet observed a clear pattern selection with a larger wavelength (e.g., 2x2-domain) in the nearest-neighbor coupling model. For larger coupling we have seen a partially ordered roll-like pattern ("labyrinth") (see Fig.11b).

3.3 Absence of a frozen pattern for stronger coupling and extension of Pierls' argument

If the coupling is further increased ($\epsilon > .4$), neither a frozen random pattern nor a pattern selection is observed. A domain is unstable and its boundary moves in time till a single domain covers the whole space.

Change of Lyapunov exponents with the parameter a is smooth, and the Lyapunov spectra have a smooth shape for all a [4]. These results are consistent with the absence of pattern selection.

The absence of frozen pattern is understood as the extension of Pierls' argument on the absence of ordered phases. The diffusive coupling tries to destroy the domain boundary between two frozen patterns. On the other hand, the motion in each domain is more stable than the boundary. To destroy a domain, a state has to pass through unstable states (recall that $x(i,j)$ has to take a value around the unstable fixed point of a logistic map), which requires some barrier. This effect leads to the preservation of a domain and the pinning of a boundary. The former strength is estimated by the surface tension as $\epsilon M^{(1-1/d)}$ for a domain of length M. The latter part is roughly independent of M, if M is large enough. For $d > 1$, a smaller domain has smaller stability. Thus for a lattice with a dimension ≥ 2, it is expected that there is an upperbound on the coupling strength beyond which a frozen domain structure (the frozen random pattern and the pattern selection) loses its stability.

From our numerical results, it is concluded that this threshold coupling lies around $\epsilon \approx .35$ for our 2-dimensional logistic lattice with the nearest-neighbor coupling.

In higher dimensions, it is expected that the frozen pattern is much harder to sustain in a short-ranged model.

4 Open Flow Models

So far we have investigated the case where the coupling is diffusive.

Another interesting version of CML is the one-way coupling model, introduced as a model for the open fluid flow:

$$x_{n+1}(i) = (1-\epsilon)f(x_n(i)) + \epsilon f(x_n(i-1)) \tag{14}$$

As has already been reported [13,14,15], the model exhibits the spatial period-doubling and selective amplification of noise. See Fig.14a) for the spatial period-doubling. After some doublings, our system goes to a turbulent state.

The model (14) is the extreme limit of the asymmetric coupling model

$$x_{n+1}(i) = (1-\epsilon)f(x_n(i)) + \epsilon[\alpha f(x_n(i-1)) + (1-\alpha)f(x_n(i+1)]$$

An important notion in the open flow model is the distinction with absolute and convective instabilities. If a small perturbation against a reference state grows in a stationary frame, it is called as "absolute instability", while if the perturbation grows only in some frame with a finite velocity, it is called as "convective instability" (see also "Co-moving Lyapunov exponent" in Appendix and [14]). In the above model, if the coupling is large, our system shows only the convective instability. For example, the stability of a homogeneous periodic state in a Galilean frame with a velocity v is calculated by

$$L(v) = (1/p)log(\prod_{i=1}^{p} f'(x_i)) + log(\frac{1-\epsilon}{1-v}) + vlog(\frac{\epsilon(1-v)}{v(1-\epsilon)}) \tag{15}$$

where x_i is the periodic orbit of a single logistic map. If $L(v)$ is positive for some velocity, our periodic state is convectively unstable. If $L(0) > 0$, it is absolutely unstable. For example, the homogeneous fixed point state $x* = (\sqrt{1+4a}-1)/(2a)$ is convectively unstable if $| f'(x*) | = \sqrt{1+4a} - 1 > 1$, and abosolutley unstable if $| (1-\epsilon)f'(x*) | > 1$.

I.S. Aronson, A.V. Gaponov-Grekhov, and M.I. Rabinovich [17] have recently investigated the above spatial period-doubling in open flow, using the renormalization group approach by Feigenbaum [63]. This procedure works if the coupling is very small, where the absolute instability occurs. They have calculated the scaling relation on the spatial interval in the period-doubling. If the coupling is larger, the instability which causes the period-doubling is not absolutely but *convectively* unstable. In this case the existence of a very small noise is essential to form the pattern [13]. Thus the scaling both with a noise and a space should be necessary.

Corresponding to the phase transitions in the diffusive coupling model, we have obtained similar phase transitions in the pattern dynamics, and a phase diagram similar to Fig.1. We have (i) flow of randomly chosen patterns (ii) flow with selected patterns (iii) transmission of defects (iv) spatiotemporal intermittency and (v) fully developed turbulent state (see Fig.14 and 15 for space amplitude plots and spacetime diagram).

The defect turbulence and transmission of defects to downflow with a fluctuating velocity are found which are triggered by its chaotic motion and interactions among defects. A source of defects is seen at the upper flow.

A novel point here is the spatial bifurcation from a homogeneous periodic state to a pattern selection (periodic state with a periodic spatial structure), and then to a turbulent state as a space goes downflow.

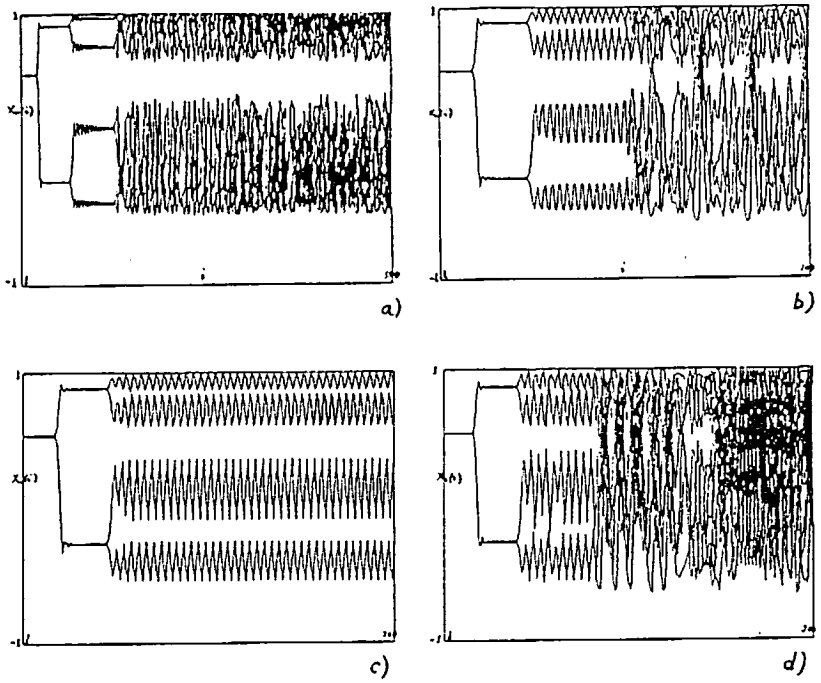

Fig.14: Space-amplitude plot for the one-way coupled logistic lattice (14). Amplitudes $x_n(i)$'s are overlayed for 250 time steps after discarding 10000 transients, starting with a random initial condition. $\epsilon = 0.5$, N=500(a), N=200 (b-d).
(a) a=1.5,(b) a=1.6 (c) a=1.63 (d) a=1.68 .

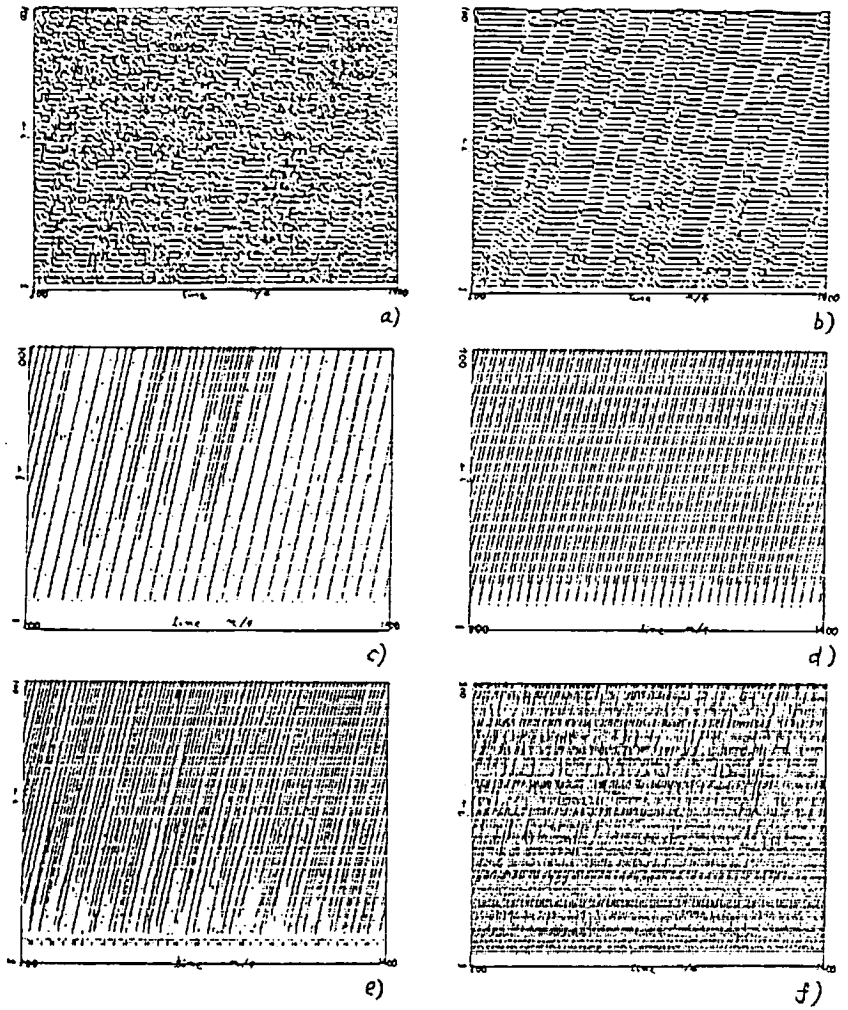

Fig.15: Space-time diagram for the one-way coupled logistic lattice with N=100 and starting with a random initial condition. Every 4th time step is plotted from 0 to 600. For the way of plotting see Fig.3. (a) a=1.58, $\epsilon = .3$ (b) a=1.6, $\epsilon = .3$ (c) a=1.63, $\epsilon = .3$ (d) a=1.75, $\epsilon = .3$ (e) a=1.83, $\epsilon = .1$ (f) a=1.86, $\epsilon = .1$.

It is rather straightforward to extend the model to a 2-dimensional case with an open flow coupling. The model is given by

$$x_n(i,j) = (1-\epsilon)f(x_n(i,j))+$$

$$(\epsilon/4)(f(x_n(i,j+1)) + f(x_n(i,j-1)) + \alpha f(x_n(i-1,j)) + (1-\alpha)f(x_n(i+1,j)). \quad (16)$$

This class of model has recently been investigated in [18,19], in a possible relation with the spatiotemporal intermittency in the open flow, and leads to some similarity with experiments of turbulence in Benard convection in Libchaber's group [64]. The transport of bursts by the asymmetric coupling in CML corresponds to the transport of hot plumes in the experiment.

5 Information Flow

Chaotic dynamics exhibits the information flow in the bit space [67]. In spatiotemporal chaos, the information flows both in real and bit spaces.

The mutual information in spacetime is useful to see the correlation in spacetime and how the information flows in spacetime. Although there are varieties of ways to see the information flow, we argue the simplest two-point mutual information in space and time, here.

First, take the two-point probability function $P(x_n(i), x_{n+t}(i+m))$, the probability that the lattice site i takes the value $x_n(i)$ at time n and the site $i+m$ takes $x_{n+t}(i+m)$. By this joint probability, the mutual information is defined as [7]

$$I^{st}(t,m;i) = \int logP(x_n(i))dx_n(i) + \int logP(x_{n+t}(i+m))dx_{n+t}(i+m)$$

$$- \int logP(x_n(i), x_{n+t}(i+m))dx_n(i)dx_{n+t}(i+m) \ . \quad (17)$$

Two extreme cases are useful: $I^t(t;i) = I^{st}(t,0;i)$, i.e., the temporal mutual information and $I^s(m;i) = I^{st}(0,m;i)$, i.e., the spatial mutual information.

In the numerical calculation of probability function we have to use a finite bin size, and replace the integral by the summation over bins. If we take the partition number M, the probability function is calculated by the bin $[-1,-1+2/M],[-1+2/M,-1+4/M],\cdots,[-1+2n/M,-1+2(n+1)/M],\cdots,[1-2/M,1]$. Although changes with the partition number M are another important characterization of a system, we study only the case with a fixed M here.

First we discuss the temporal mutual information flow. In Fig. 16, examples are shown. For the frozen phases (frozen random pattern and pattern selection), the mutual information $I^t(t;i)$ depends on sites (Fig.17a). For the fully developed turbulent phase, the function is independent of sites (Fig.17b), showing the *spatial ergodicity*. The exponential decay is seen. The rate of this decay decreases as the nonlinearity is decreased, till it goes to zero at the intermittency transition. The decay is roughly fitted by the power-law decay in the critical region. In the frozen regime, the decay of information stops at some value (Fig.17a), as far as the precision M is finite, since there is a period-2 peak in the power spectrum. The site dependence of the mutual information clearly shows that the chaotic motion is different by sites.

Spatial mutual information is shown in Fig.18. We again note that the decay is exponential in the fully developed turbulent phase, whose rate of decay decreases as

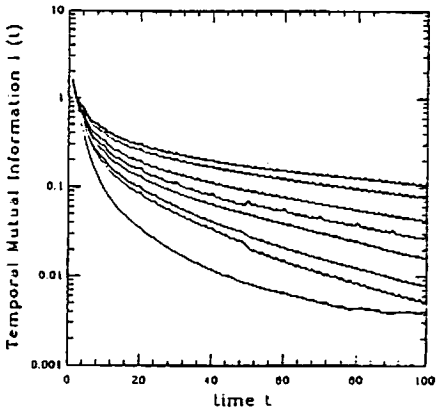

Fig. 16: Temporal mutual information flow for the logistic lattice (1): calculated using the bin number $M = 64$, and 500000 time step sampling, after discarding 100000 step transients. $N = 100$, $\epsilon = .3$. a =1.78, 1.79, 1.8, 1.81, 1.82, 1.83, 1.84, and 1.88 from top to bottom. The site dependence is small here as is seen in Fig.17b).

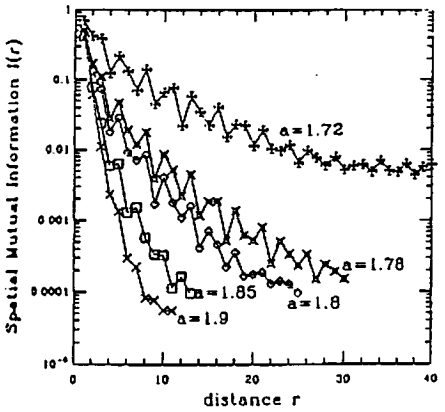

Fig. 18: Spatial mutual information flow for the logistic lattice (1): calculated using the bin number $M = 64$. Probability is sampled from 5000 time steps after 100000 steps, and throughout the whole lattice. $N = 500$, $\epsilon = .3$. a = 1.72, 1.78, 1.8, 1.85, and 1.90 from top to bottom.

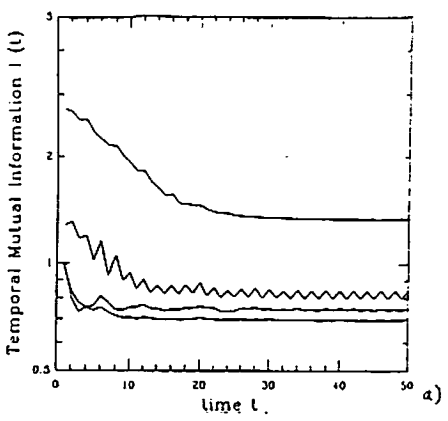

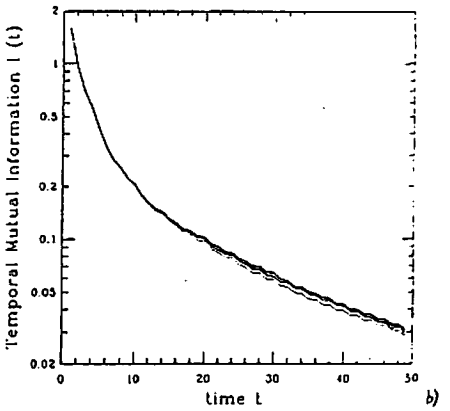

Fig. 17: Temporal mutual information flow calculated in the same manner as in Fig.16. Results from 4 successive lattice points are overlayed. (a) $a = 1.77, \epsilon = .3$ (b) $a = 1.83, \epsilon = .3$.

the parameter approaches the transition point. We also note that a smaller periodic change is added in the mutual information, which comes from the spatial domain structure. Indeed, the wavelength in this smaller variation (Fig. 18) agrees with that of the selected pattern in §2.

The mutual information $I^{st}(t, t/v; i)$ is called as co-moving mutual information flow and gives the measure how the information (or coherence) propagates with the speed v. This measure is especially important in the open-flow model [7].

6 Thermodynamics

In low-dimensional chaos, the statistical mechanics theory has been developed. The essence of statistical mechanics can be seen in Ruelle's textbook[68]. The study of this direction has been developed by I. Shimada, K. Tomita, T. Kai,[70] Y. Oono, Y. Takahashi,[69] and so on, before it has become suddenly popularized in recent days.

According to these works, the chaotic dynamics can be mapped to the statistical mechanics of a 1-dimensional spin system.

Then, it is natural to expect that the thermodynamics of our k-dimensional CML can be mapped onto the statistical mechanics of $k+1$-dimensional spin systems. The interaction, of course, is strongly anisotropic, since the interaction in "spatial" directions is short ranged and bidirectional (e.g., nearest neighbor), but the interaction in "temporal" direction is unidirectional and has a more complicated longer ranged form.

Quite recently Bunimovich and Sinai have rigorously constructed the statistical mechanics corresponding to CML for a special case [24].

Another approach in a different direction has recently been carried out by the author, where the self-consistent approximation on the Perron-Frobenius operator has been formulated. Here it is briefly explained.[25]

The Perron-Frobenius (PF) operator has been a powerful aid in the study of the statistical mechanics of low-dimensional chaos [68,69,71]. The operator has first been extended to spatially extended systems by [72], where the local structure theory of cellular automata is constructed. The operator for the entire dynamical system acts on the measure on N-dimensional space $\rho(x(1), \cdots, x(N))$. The operator is written as

$$H^{PF}\rho(x(1), \cdots, x(N)) = \sum_{y(i)=preimages} \frac{\rho(y(1), \cdots, y(N))}{J(y(0), \cdots, y(N-1))} \tag{18}$$

where the sum takes over all possible sets of $(y(i))$, preimages of $x(i)$ (i.e., $y(i) \to x(i)$ by the map (1)) and $J(y(0), \cdots, y(N-1))$ is the Jacobian of the CML transformation (1).

In our model, the preimages are easily calculated, since it consists of two separated procedures, i.e., $y(i) \to x'(i) = f(y(i))$ and the spatial average by $x(i) = (1-\epsilon)x'(i) + (\epsilon/2)(x'(i+1) + x'(i-1)) \equiv \sum D_{i\ell}x'(\ell)$. The inverses of these two processes are just given by $f^{-1}(x)$ (for the logistic map $f^{-1}(x)$ is given by $\pm\sqrt{(1-x)/a}$) and the inverse matrix D^{-1}.

Since the treatment of N-dimensional distribution is practically impossible, we use a projection to a low-dimensional space. There are many possible ways of the projection. We use the simplest projection here, that is a projection to a k-dimensional space $x(1), \cdots, x(k))$, by intergating out other variables. To get a closed equation within a k-dimensional space, we need a truncation of probability function. It is a traditional

problem in statistical mechanics, and various elaborated methods have been developed. Here we use the simplest approximation, that is, the self-consistent approximation. Following this method and after some calculations [25] we have

$$H^{SPF}\rho(x(1), x(2), \cdots, x(k)) = (detD'(k))^{-1} \int\int \sum_{y(1),\cdots,y(s)} dy(0)dy(k+1)$$

$$\frac{\rho(y(1), \cdots, y(k))P(y(2), y(3), \cdots, y(k)|y(k+1))P(y(1), y(2), \cdots, y(k-1)|y(0))}{\prod_{j=1}^{k} |f'(y(j))|} \tag{19}$$

where the conditional probability P is given by

$$P(y(2), y(3), \cdots, y(k)|y(k+1)) = \rho(y(2), y(3), \cdots, y(k), y(k+1))/\rho(y(2), y(3), \cdots, y(k)) \tag{20}$$

and the preimages $(y(1), y(2), \cdots, y(k))$ are given by the solution of

$$y(j) = f^{-1}(D'^{-1}_{j,\ell}(k)x_\ell - (\epsilon/2)(f(y(0))\delta_{j,1} + f(y(k+1))\delta_{j,k}) \,. \tag{21}$$

The matrix $D'(k)$ is the diffusion matrix D_{ij} of size k without a periodic boundary (i.e., $(1-\epsilon)\delta_{i,j} + (\epsilon/2)(\delta_{i+1,j} + \delta_{i-1,j})$).

We have applied this self-consistent method with $k=1$ and $k=2$ to the problem of spatiotemporal intermittency transition from a laminar regime to a turbulent regime. As for the transition point, the above approximation gives a reasonable result (within 10 % error).

7 Mean-field Type Model

The above self-consistent equation is *different* from the mean-field theory. The mean-field-type model (Fushimi-Temperley-type model) is constructed as a model with couplings to all other elements. The model corresponding to our diffusively coupled map lattice is written as

$$x_{n+1}(i) = (1-\epsilon)f(x_n(i)) + (\epsilon/N)\sum_{j=1}^{N} f(x_n(j)) \,. \tag{22}$$

The above model has a remarkably rich behavior (partly similar but much richer than Sherrington-Kirkpatrick (SK) model[83] as a mean-field model for spin-glass).

The model here exhibits the phase transition among a coherent phase, an ordered phase, a glassy phase, an intermittent phase, and a turbulent phase, as the nonlinearity is increased. Also it turns out that the glassy phase and intermittent phase have attractors of similar tree-like structures as are investigated in the SK model. The important difference here is that our tree structure is dynamically changing. Coding of these attractors and switching among attractors are discussed in [43].

8 Simulating Science with Coupled Map Lattices

Our strategy of studying dynamical phenomena in spatially extended systems by CML is based on the separation of parallel procedures and successive operations of them (§1).

In the previous diffusively coupled model, the independent procedures are local transformation of $x(i)$ by a simple 1-dimensional map (eq.(2)) and the diffusion process (eq.(1)), given by the discretized Laplace equation. These two procedures are separated and successively carried out.

If we are interested in phenomena described by local nonlinear processes with local spatial coupling, it is possible to use the above procedures.[8]

8.1 Pattern formation (spinodal decomposition)

Understanding the pattern formation process is the main topic of the present book.

A typical and interesting problem is spinodal decomposition, [74,49] which is a phenomenon when a system is quenched from a disordered state to an ordered state. Traditionally this problem is studied by the time-dependent Ginzburg-Landau equation or the kinetic Ising model with Monte Carlo method.

Oono and Puri have proposed a CML for this problem, which is one of the best success among the applications of CML [27]. Their model is based on the coarse graining in a cell with a large number of sites from the kinetic Ising model. Then the local dynamics of a cell leads to a map with two stable fixed points, e.g.,

$$f(x) = \tanh(\beta x) \ . \tag{23}$$

The same diffusive coupling form as in the previous sections can be used since the phase transition dynamics includes the term which tries to make two neighboring regions to order ("ferro-coupling").

In the above model the order parameter $\sum_{i,j} x_n(i,j)$ is not conserved. If the order parameter is conserved, the established method in the kinetic Ising model is the use of Kawasaki's exchange dynamics[49]. Corresponding to this class of dynamics, it is possible to construct a CML with the constraint $\sum x_{n+1}(i,j) = \sum x_n(i,j)$ [27]. The model with this constraint is written as

$$x_{n+1}(i,j) = f(x_n(i,j)) - << f(x_n(i,j)) - x_n(i,j) >> \tag{24}$$

where $<< \ldots >>$ denotes the spatial average with the nearest neighbor.

The models by Oono and Puri give correct scaling behaviors for dynamical form factors (⇒ Appendix) corresponding to the conserved and non-conserved phase transition dynamics, respectively. Indeed, their models give much faster simulators than the conventional Monte Carlo method.

8.2 Other pattern formation problems

A similar modelling is possible in the roll formation in convection, pattern formation with complex order parameter(s), and so on. These extensions are rather straightforward. Vortex interactions in the Ginzburg-Landau equation are easily simulated with the use of vector order parameter $\vec{x}_n(i,j)$ and the similar local dynamics as (23) and the same diffusive coupling [28]. Another application is the complex Ginzburg Landau

[8] "local" here means that the interaction is governed by a term decaying exponentially (or faster) in space. Thus we may hope that our method is applicable to a system of reaction-diffusion type equation (including time-dependent Ginzburg-Landau equation), and most spatially extended dynamical phenomena.

equation with complex parameters [75], in which a turbulent behavior with vortices is observed [29,30].

Formation of a roll pattern is also simulated by CML. So far we have two modellings on the roll formation. One is the use of $f(x)$ which is an odd function and has a maximum at $x = x_c$ and goes to zero as $x \lim \infty$. An example is

$$f(x) = G((3\sqrt{3}/2(x/x_0 - (x/x_0)^3), G(y) = y/\sqrt{a^2 + x^2} \tag{25}$$

with same diffusive coupling form as in (1)[29] (see Fig.19). The other method is the use of a "lateral" inhibition in the next-nearest-neighbor coupling[31]:

$$x_{n+1}(i,j) = (1 - n_1\epsilon_1 + n_2\epsilon_2)f(x_n(i,j)) + \epsilon_1 \sum_{n.n} f(x_n(i',j') - \epsilon_2 \sum_{n.n.n} f(x_n(i'',j'')) \tag{26}$$

where $n.n.$ is the sum over nearest neighbors whose number is n_1, while $n.n.n.$ is the sum over next nearest neighbors whose number is n_2. By choosing the couplings suitably, we can have a model of a roll formation.

It is rather straightforward to apply these methods with different classes of ordered patterns and order parameters.

8.3 Crystal growth

Another possible application lies in the nucleation and crystal growth [76]. To take into account a thermal field, it is possible to introduce the following model:

$$x_n(i,j) = (1-\epsilon)f(t_n(i,j), x_n(i,j)) + (\epsilon/4)[f(t_n(i,j+1), x_n(i,j+1)) +$$
$$f(t_n(i,j-1), x_n(i,j-1)) + f(t_n(i-1,j), x_n(i-1,j)) + f(t_n(i+1,j), x_n(i+1,j))] \tag{27}$$

$$t'_n(i,j) = t_n(i,j) + c(f(t_n(i,j), x_n(i,j)) - x_n(i,j)) \tag{28}$$

$$t_{n+1}(i,j) = 1/n_{nghbr} \sum_{nghbr} t'_n(i,j) \tag{29}$$

with $f(t,x) = tanh(\beta(x-t))$.

Here x denotes the order parameter corresponding to the density ($x = 1$ is solid, $x = -1$ is gas). The other variable t corresponds to the temperature field. Threshold on the solidification process is clearly seen in the form of $f(t,x)$. The equation $t \rightarrow t'$ represents the effect of latent heat by the solidification. Eq. (29) comes from the diffusion of heat, where $\sum_{nghbr}$ shows the summation over given neighbors, and n_{nghbr} is their number. A simple examples of a growth of a "solid" region is shown in Fig.20. The growth consists of the repetition of the process in the figure.

8.4 Excitable media

Another possible application of CML is a model with an excitable state and a relaxation from it. Possible examples can be seen in reaction diffusion within excitable media, and may also be relevant to some problems of neural response.

A simple 1-dimensional map with an excitable state is introduced by Nagumo and Sato[77], in connection with Harmon's experiment on the firing of an artificial neuron [78]. They have used the map

$$f(x) = b \times (x - H(x)) + c \tag{30}$$

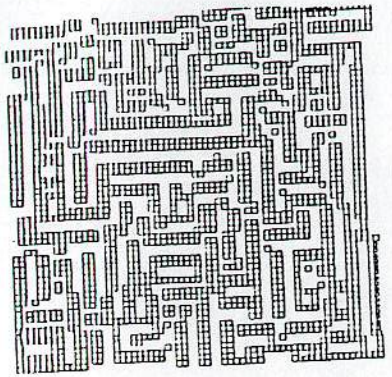

Fig. 19: Roll pattern formation. Snapshot of the diffusively coupled map lattice (25). Size = 64x64. $a = 1/4$, $x_0 = 0.8$, and $w = 0.8$, at the time step 4000. Nearest-neigbor average for diffusion. Squares are depicted only at the points (i, j) with $x(i, j) > 0$ whose length are proportional to $x(i, j)$.

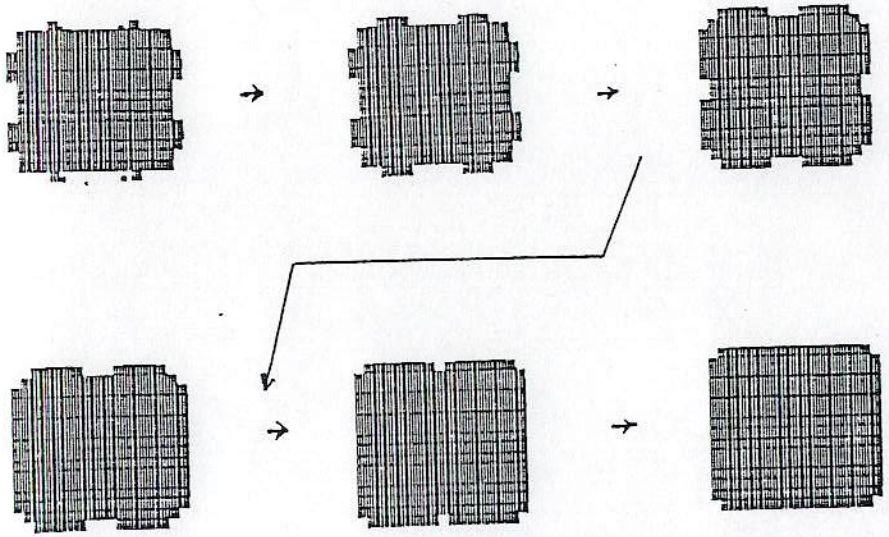

Fig. 20: Crystal growth model (27)-(29). Snapshot of $x(i, j)$, with $\beta = 3.5$, $c = -.55$, starting from a 3-site-seed initial condition. Nearest-neighbor average for diffusion. Only the points with $x(i, j) > 0$ are painted by square whose length is proportional to $x(i, j)$.

where $H(x)$ is the Heaviside's step function ($H(x) = 1$ for $x > 0$ and $H(x) = 0$ for $x < 0$). Here, $x > 0$ corresponds to the " fired state". The constant term "c" comes from an external stimulus applied on a single neuron [77].

We can easily construct a CML corresponding to the above model. If we follow the interpretation of the term "c", we can replace this constant term by stimuli from other lattice points. As a simple model, we assume that a constant pulse is emitted if $x > 0$ ("fired"). Then we obtain the following CML

$$x_{n+1}(i) = b \times (x_n(i) - H(x_n(i))) + d \times (H(x_n(i+1)) + H(x_n(i-1)) \quad (31)$$

(for a 1-dimensional lattice) or

$$x_{n+1}(i,j) = b \times (x_n(i,j) - H(x_n(i,j))) +$$

$$d \times (H(x_n(i+1,j)) + H(x_n(i-1,j)) + H(x_n(i,j+1)) + H(x_n(i,j-1))) \quad (32)$$

for a 2-dimensional lattice.

In the 1-d lattice, we can see the propagation of pulses. At a transition parameter region we can see a soliton turbulence induced by the interaction among pulses [35].

In the 2-dimensional system, we have observed the wave pattern similar to the experiment of BZ reaction. See Fig. 21 for examples.

It will be of use to study a system with more realistic couplings and local functions.

8.5 Dripping handrail and boiling chaos

Another related model is a system with a threshold dynamics and diffusion. As an example of a 1-d lattice, let us take a dripping handrail [5,23]. Water comes from the rain onto a handrail and the amount of water increases with a constant rate up to a threshold. If the amount exceeds the threshold, the water drops from the handrail. These two processes give the local dynamics. There is diffusion along the handrail, which can be modelled by the diffusive coupling. Thus we have $x_{n+1}(i) = (1-\epsilon)f(x_n(i)) + (\epsilon/2)(f(x_n(i-1)) + f(x_n(i+1)))$ with

$$f(x) = x + c(mod\ 1). \quad (33)$$

The spatiotemporal chaos here is of a different nature from that discussed in §2-7, since the model cannot have a state with positive Lyapunov exponents as an attractor. The model exhibits the supertransients [23]. The duration of transients increases with a system size, and a quasistationary chaotic behavior is seen in this transient interval. An extension to a 2-dimensional system is straightforward [32]. The 2-dimensional model may be regarded as a simple model for boiling, since the boiling process consists of the increase of temperature up to a threshold and diffusion.

8.6 Designing fluid dynamics with CML?

One difference between Navier-Stokes-type equations and our diffusively coupled map lattice lies in that the nonlinearity in the former arises from the coupling term as is typically seen in the convective term in the Navier-Stokes equation, while in the diffusively coupled model, the coupling term acts as a smoothing effect. Here we

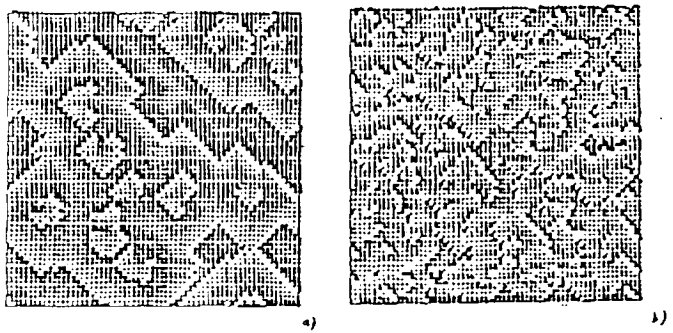

Fig. 21: Snapshot for a CML model for the excitable media model (32). $b = .77$. Time step =1000, starting from a random initial condition. A length of a side of a square in the figure is proportional to $x(i,j) + .5$. If $x(i,j) < -.5$, the corresponding site is left blank. Size=64x64. (a) $d = 0.06$ (b) $d = 0.1$

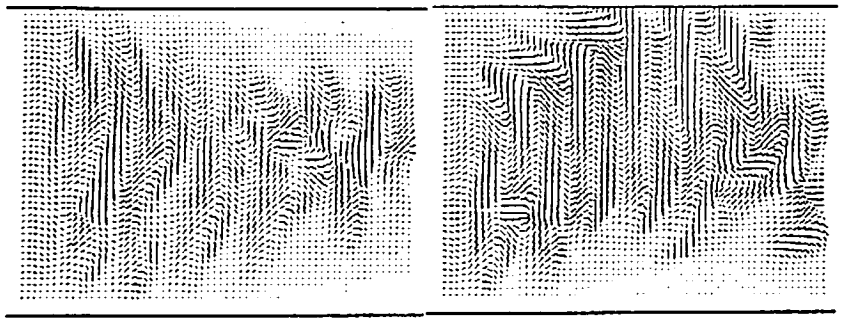

Fig. 22 a) b)

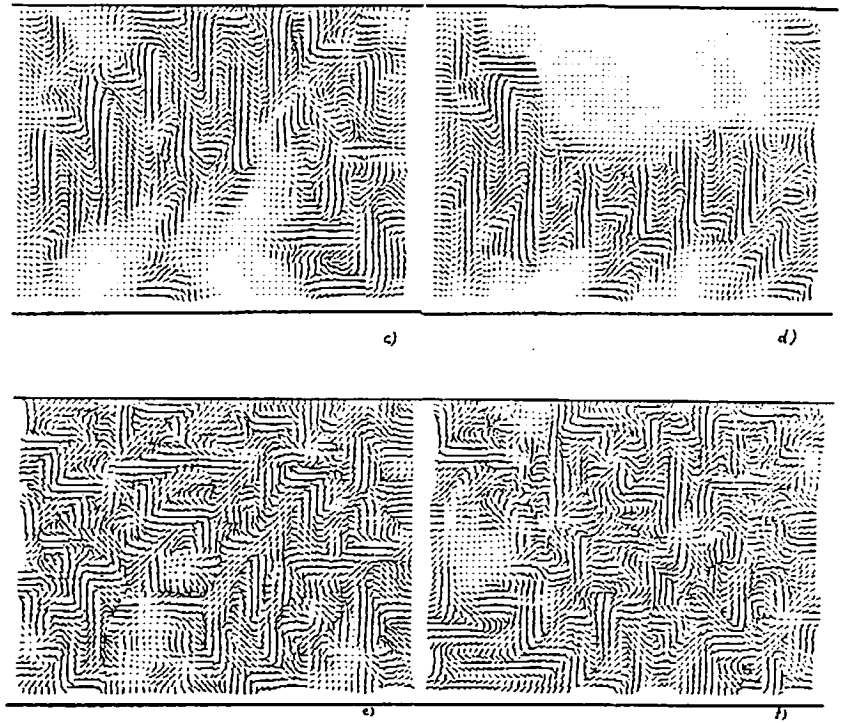

Fig. 22: Snapshot for the 2-dimensional convective coupling model (37)-(39): Left boundary is fixed at $(x, y) = (v_L, 0)$ and right boundary is free. Top and bottom are rigid, i.e., $(x, y) = (0, 0)$. Lattice size is 63x48.
(a) $v_L = 2.3$, $c = 130$, time step =2081
(b) $v_L = 2.5$, $c = 130$, time step =705
(c) $v_L = 3.0$, $c = 200$, time step =225 (d) time step =353
(e) $v_L = 2.2$, $c = 300$, time step =1345 (f) time step =3585

consider a model with nonlinear coupling, which has some similarity with a turbulent behavior in Navier-Stokes-type equations.

soliton turbulence in a convective coupling model

As a simple example for a convective coupling model, let us take the following procedures.

(1) Convective coupling (corresponding to the $-(v\nabla)v$ term in the Navier-Stokes equation)

(2) Diffusive coupling (corresponding to the $\nu\nabla^2 v$ term in the Navier-Stokes)

(3) Cut-off for high velocities: (this term is rather artificial but necessary in order to remove a possible divergent behavior). A simple example is given by $x'(i) = f(|x(i)|) * x(i)$ with a monotonically decreasing function $f(x)$ with $f(0) = 1$ and $f(\infty) = 0$. Here we take $f(x) = exp(-x^2/c)$.

Combining these three procedures, our coupled map lattice is given by

$$(I)x'(i) = x_n(i) + (x_n(i-1) - x_n(i+1))x_n(i) \tag{34}$$

$$(II)x''(i) = (1-\epsilon)x'(i) + \epsilon/2(x'(i-1) + x'(i+1)) \tag{35}$$

$$(III)x_{n+1}(i) = exp(-x''(i)^2/c)x''(i)\ . \tag{36}$$

The evolution $x_n(i) \rightarrow x_{n+1}(i,j)$ consists of the successive operations of the procedures (I),(II), and (III).

This model includes two parameters $1/c$ and ϵ, corresponding to the damping and diffusion. As c is increased, the system starts to explore a region with larger nonlinearity. With the increase of c, our attractor changes as follows; (i)"dead" state (i.e., $x(i) = 0$ for all i) $\rightarrow$ (ii)soliton turbulence $\rightarrow$ (iii) developed turbulent state.

The soliton turbulence is a turbulent behavior generated by the transmission of "solitons" and their interaction and creation. The interaction consists of the emission of solitons from a chaotic nucleus, and collisions which result in pair-annihilation, absorption, passing-through with a phase shift, and a generation of a nucleus. There is sensitive dependence on the phases of collisions.

The soliton turbulence is first found in the coupled circle lattice [11,5] and is also seen in a class of cellular automata [50,52].

2-dimensional flow

The above model is straightforwardly extended to a flow in a two-dimensional system, by taking a two-dimensional vector $\vec{v}(i,j) = (x(i,j), y(i,j))$ instead of the scalar quantity on a 2-dimensional lattice (i,j). The model consists of the following successive procedures.

$$(I)'x'(i,j) = x_n(i,j) + [(x_n(i-1,j) - x_n(i+1,j))x_n(i,j) + (y_n(i,j-1) - x_n(i,j+1))x_n(i)]/2 \tag{37}$$

$$(I)'y'(i,j) = y_n(i,j) + [(x_n(i-1,j) - x_n(i+1,j))y_n(i,j) + (y_n(i,j-1) - x_n(i,j+1))y_n(i)]/2 \tag{38}$$

$$(II)'x''(i,j) = \text{average of } x'(i,j) = \text{for 13 neighbors } ((i\pm1, j\pm1), (i\pm2, j), (i, j\pm2))$$

$$(III)'x_{n+1}(i,j) = x''(i,j)exp(-(x''(i,j)^2 + y''(i,j)^2)/c)\ . \tag{39}$$

(Procedures for $y(i,j)$ are similar.)

Examples of snapshots are shown in Fig.22, where the boundary condition is fixed at the left end and free at the right end, while it is fixed to zero at the top and bottom. We can see the formation of shocks, vortices, sinks, and sources (since we have not imposed the "incompressibility" condition in our model).

PROBLEM: We have to admit that the model (I)'-(III)' is still a premature attempt towards a modelling of hydrodynamics, compared with the expanding field of lattice gas automata [46]. Drawbacks in our model lie in the existence of artificial cut-off term (III) and a very rough treatment of the conservation law. In fact, our model has a conservation law only in the limit of small diffusion ($\epsilon \rightarrow 0$) and $c \rightarrow \infty$. One possible refinement of our model is to introduce another quantity corresponding to the density and to take into account of a discrete version of the equation of continuity. Or, another choice is to start from the coarse-graining of microscopic dynamics without any direct consideration of the Navier-Stokes equation.

Without the cut-off term (III)', an interesting behavior is observed only at a critical point in the parameter space. Beyond this point, our model shows a divergent behavior, while below it, the system goes to a laminar flow. It will be important to search for a mechanism to compel to stay near the critical point by a conservation law, as has been discussed in the model of sandbox by [79].

8.7 Neural networks

In the real neuron, states are not discrete. In that sense the discrete-state model of a neural network (e.g., McCllough-Pitts neuron) is an over-simplification. Of course, the model may capture some essential features of the neural dynamics, but may miss some important points, too. In some experiments, a single neuron [80,81] and a small ensemble of neurons [82] are known to exhibit a chaotic behavior. In the standpoint of statistical mechanics, it must be much better to start from a higher-level dynamics than the neural networks with very simple elements, in order to understand a higher-level dynamics in the brain.

Thus it is natural and important to ask the following question: What happens if we use more complex elements (with a chaotic response) with oversimplified couplings instead, as a different limit of simplification from the neural dynamics? The coupling here is not short-ranged.

The global coupling model in §7 may be of importance as the first endeavor towards this direction. The results there [43] are rather promising. We can have a huge number of coded attractors. Some attractors have a tree-like structure with a hierarchical code and have similar complexity with the SK model in spinglass [83], which is the basis of one of the most popular models in neural networks [84,85,86]. Upon the tree structure one can construct a hierarchical dynamics. Through simple inputs on coded attractors, we can switch from them to attractors with different clusterings and tune the strength of chaos.

It is of course interesting to study a CML with local dynamics with an excitable state and a refractory period, and with a coupling which gives the transmission of the firing. A possible example is the use of the model discussed in §8.4, and with a different topology ([35], see also [36]).

8.8 Josephson junction, CDW, ... and coupled circle lattice

The problem of coupled nonlinear oscillators (pendula) can be frequently seen in the solid-state physics. Typical examples include a Josephson junction and a charge density wave (CDW).

Since a forced pendulum can be well modelled by the circle map $f(x) = x + (K/2\pi)sin(2\pi x) + \Omega$ (see e.g., [2]), it is natural to use a coupled circle map lattice for the above problems.

Some preliminary results in the coupled circle map lattice give a soliton turbulence [11,5] and a vortex motion in a 2-d lattice[11]. See [33,34] for applications of these models to problems of CDW. In [42], a problem of a coupled Josephson junction is investigated with the use of a globally coupled circle map, where a transition from a coherent state to a desynchronized state is studied.

Another approach towards this problem is seen in the use of "oscillator lattice", that is a coupled ODE with the use of a differential equation of an oscillator as a local dynamics. [87,88].

8.9 Other applications

Recall that the logistic map has frequently been investigated as a problem of population dynamics. Then it is natural to ask the role of spatial interaction among the populations. Coupled logistic lattices and some other models will be of importance for the study of this problem[37].

The oscillatory behavior of immune response also includes a large number of nonlinear interactions. A possible model for immune networks with a CML is discussed in [90].

8.10 Experimental observation of spatiotemporal chaos

We comment briefly on the possible relation of our logistic lattice with experiments. First, we have to admit that the direct relation with an experiment is not attainable at the present. We do not have to be disappointed with this, however, since no direct relation with the logistic map and a Rayleigh-Benard convection is at hand in the level of equation of motion, but the map explains some aspects of the latter quite well. If the universality class to which our model belongs has a large applicability in the spatiotemporal chaos, which we believe (since our model is so simple and general like the Ising model or the logistic map), we might hope that the same phenomena and quantitative aspects as in our CML are observed in experiments.

We also note that the "universality" is not necessarily defined quantitatively (like critical exponents which we are not interested in). It will be important to define the universality in a qualitative level. For examples, if we have experimentally observed the transition sequence of pattern dynamics similar to our model, we may say that the experiment belongs to the same qualitative universality class as our model.

What we hope to be observed is (1) the transition sequence of the frozen chaotic pattern, the pattern selection, the intermittency (Brownian motion of defect and the defect turbulence), and the fully developed turbulence. If this kind of phenomena is found, the search for (2) selective flicker noise at the transition regime is recommended as a quantitative check. Also, it is desirable to re-investigate (3) the motion of defects in some patterns, to check if the motion is chaotic, and if the Brownian motion is associated with the chaos.

For a qualitative comparison, some visualization techniques introduced in the study of CML, such as the space-time diagram, spatial return maps, co-moving return maps and so on [5] may be useful. For these qualitative and quantitative studies, multiple-point observations will be essential. Through these observations, we can get the graphics and various quantifiers comparable with those investigated in the present paper.

What are possible candidates of the experiments? We have seen some examples of spatiotemporal chaos in recent experiments [89], such as chemical turbulence [91, 92], Benard convection with large aspect ratio [93,94,95,96,97], Taylor-Couette flow with large aspect ratio [98], Faraday experiment [99] electrical convection of liquid crystal [100,101], solid state experiments such as Josephson junction array, electron-hole plasma [102], and charge density wave [103]. For open flow experiments, we have seen many examples of spatiotemporal chaos, such as the pipeflow [104], boundary layer [105], and air jet [106], and the dendritic growth of a crystal [107].

In these experiments, we can see some relations with our observations in the present paper. Spatial bifurcation by the frozen random state is observed in a Benard convection experiment [97]. Brownian motion of defects has been seen in the convection of liquid crystals. Localized chaotic motion (turbator) has been observed in Taylor-Couette flow [98]. Pattern competition is observed in the Faraday experiment and in liquid crystal experiment [99,101]. Flow of turbulent spots can be frequently seen in open flow experiments and in a dendritic growth [107].

Spatiotemporal intermittency has been observed by Ciliberto and Bigazzi [108] on the Benard convection on an annulus. The experiment exhibits the same phenomena as our pattern competition intermittency. This correspondence is supported by the power-law distribution of laminar domains, and the existence of selected wavenumbers and of localized chaos in a subcritical region.

Another important experiment has been carried out by Nasuno et al.[62], in the electrical convection of a liquid crystal. As has been discussed in §3, their experiment shows a remarkable coincidence with our spatiotemporal intermittency.

If we are concerned with an experiment on a phenomenon which includes a local chaotic mechanism and a spatial short-ranged coupling, we may hope, at a level of qualitative "universality', that our prediction on the phases and the quantitative aspects is valid to the experiment.

to conclude ...?

Are all macroscopic dynamical behavior with many degrees of freedom modelled and understood by CML? I hope that the answer is no, but so far there is no counter-example....

Acknowledgement

I would like to thank Professor Kyozi Kawasaki for his continual encouragement, valuable comments, and interests on CML since I had started it several years ago. I am also grateful to him for his giving a chance to talk in the workshop on pattern dynamics in Kyoto and to write in the present book. I would also like to thank Dr. T. Ikegami for useful discussions.

9 Appendix: Quantifiers in Spatiotemporal Chaos (in alphabetical order)

Co-moving Lyapunov spectra

The notion of a co-moving Lyapunov exponent is useful, if a disturbance grows with a characteristic velocity or if macroscopic structures propagate. The co-moving Lyapunov exponent is especially important when a system is convectively unstable, as is seen in the one-way coupled logistic lattice (see §4).

The definition of the convective instability is as follows: Let us take a small perturbation δx_n^i around a state x_n^i. If $\lim_{\delta x_0 \to 0} \lim_{n\to\infty}(\delta x_n^i/\delta x_0) \to \infty$ for an arbitrary fixed lattice site i, it is called absolutely unstable. This definition agrees with the familiar definition of the conventional dynamical system theory. In a case of open flow, even if the system is not absolutely unstable, it can be unstable in some moving frame. If $\lim\ (\delta x_n^{[i+vn]}/\delta x_0) \to \infty$, for a given velocity v, it is called as convective unstable. (Here, [q] is the maximum integer that is smaller than q.) If a system is stable in all arbitrary moving frames, it is absolutely stable. The notion of convective instability was originally introduced in the field of plasma physics and fluid mechanics, where the stability around a stationary state (fixed point or periodic orbit in the terminology of a dynamical system) has been investigated.

The convective (in)stability around any arbitrary state is analyzed by the notion of co-moving Lyapunov exponent. It is defined in the following way: First, the frame is transformed from the stationary laboratory frame to the moving one. In our lattice system the transformation is given by

$$i\prime = i - [vn] \tag{40}$$

where i and $i\prime$ are spatial lattice points (in the stationary and moving frame, respectively) and n is the discrete time step. The Lyapunov exponent in the moving frame with the velocity v is calculated from the Jacobi matrix $J_n = \delta x_n^{i\prime+[v(n+1)]}/\delta x_n^{i\prime+[vn]}$. A logarithm of the largest eigenvalue of the product of Jacobi matrices divided by the time steps, gives the co-moving Lyapunov exponent with the velocity v.

When a system is only convectively unstable, the conventional Lyapunov exponent is negative, while it takes a positive value for $v_T < v < v_L$. It goes negative again for $v > v_L$, meaning that the disturbance cannot propagate with the velocity larger than v_L. Here the subscripts T and L stand for trailing and leading, and these are appropriate since these speeds describe the trailing and leading edge propagation of amplified perturbations, respectively.

Co-moving mutual information flow

see §5 and [7].

Dimension density

The fractal dimension of an attractor in the phase space is an important quantity. Roughly speaking, its integer part gives the effective degrees of freedom of the attractor. Whereas the Lyapunov dimension is introduced by the Kaplan-Yorke formula;

$$D_L = j + (\sum_{i=1}^{j} \lambda_i/|\lambda_{j+1}|) \tag{41}$$

with j such that $\sum_{i=1}^{j} \lambda_i > 0$ and $\sum_{i=1}^{j+1} \lambda_i < 0$. The Lyapunov dimension gives the upperbound to the fractal dimension of a dynamical system.

In the lattice system, a quantity scaled by size is more relevant. The Lyapunov dimension density is defined by $d_L = D_L/N$. See [38] for a possible estimate of dimension density.

These definitions are introduced in the same manner as in the introduction of "intensive" quantities from "extensive" quantities in thermodynamics.

Dynamical form factor (Spatiotemporal power spectra)

Power spectra in time and space are defined by

$$P(k,\omega) = << |(1/N)\sum_{j=1}^{N} x_n(j)e^{2\pi i(jk-n\omega)}|^2 >>, \tag{42}$$

where the bracket << .. >> denotes the long-time average. These are useful in the characterization of space-time patterns.

Kolmogorov-Sinai entropy density

Originally, Kolmogorov-Sinai (KS) entropy means the increasing rate of a variety of possible symbol sequences generated by the dynamics, with the increase of a partition precision. It can be numerically computed by the sum of all positive Lyapunov exponents (⇒*Lyapunov Spectra*). It roughly gives the information loss in the phase space.

In a spatially extended system, the KS entropy is proportional to the system size, when the spatial correlation length is finite. Thus the KS entropy density is defined as the *intensive* thermodynamic quantity:

$$h_\mu = (1/N)\sum_{i=1}^{\lambda_i>0} \lambda_i. \tag{43}$$

Lyapunov spectra

The Lyapunov exponents characterize how a set of independent small deviations in a tangent space is amplified (or reduced). In a N-dimensional dynamical system, there exist N independent directions, and corresponding N eigenvalues, which form the spectrum.

In our coupled map lattice system, Lyapunov spectra can be defined in the following by using the product of Jacobi matrix of the map, i.e.,

$$\lim_{n\to\infty} (1/n) J_n J_{n-1} J_{n-2} J_1 \ . \tag{44}$$

The logarithm of eigenvalues of the above product divided by time steps n with the limit of $n \to \infty$ gives the Lyapunov exponents. The exponents λ_i, ordered from the largest to the smallest, gives a spectrum of the system.

If the largest Lyapunov exponent takes a positive value, two nearby orbits separate exponentially, and the system exhibits the orbital instability, or in other words, sensitive dependence on initial conditions. If the largest one is negative, the orbit is stable and the system is attracted to a periodic state. If the largest one is zero, the motion is quasiperiodic. If there are k vanishing exponents, the motion is on a $(k+1)$-torus.

Corresponding eigenvectors to each eigenvalues of the matrix (44) are called Lyapunov vectors.

Mutual information in spacetime

see §5.

Pattern dynamics quantifiers

(a)Pattern distribution Q(j) and pattern entropy

Since the spacetime patch $x_n(i)$ has too much information, it is useful to reduce the information by a coarse-grained measurement of the continuous variables into some discrete states. Here we digitize a spatial pattern as a symbol patch. We first assign $\sigma_n(i) = 0, 1, 2, \cdots, K-1$ to $x_n(i)$ according to the following rule

$$\begin{aligned} &\sigma_n(i) = 0 \quad if \quad x_n(i) < X_1 \\ &\sigma_n(i) = 1 \quad if \quad X_1 < x_n(i) < X_2 \\ &\cdots \\ &\cdots \\ &\sigma_n(i) = K-1 \quad if \quad X_{K-1} < x_n(i) \ . \end{aligned} \tag{45}$$

The simplest digitization K=2 is carried out by the symbolization $\sigma_n(i) = 0$ for $x_n(i) < x*$ and $\sigma_n(i) = 1$ for $x_n(i) > x*$. In the domain structure we study in §2, each domain is separated by the separatrix of the unstable fixed point of the logistic map $x* = (\sqrt{1+4a} - 1)/(2a)$. Thus a snapshot pattern can be represented by a symbol sequence such as $0111\cdots001$.

Order parameter for the pattern selection is constructed by the domain distribution. A domain in §2 is defined as the maximal continual sequence in which $\sigma_n(i)$ takes the same value. Thus the probability distribution $Q(j)$ of the spatial length of the same symbol ($11\cdots11$ or $00\cdots00$) is chosen as the order parameter(s) for our pattern dynamics. $Q(j)$ is defined by the following procedure: From the spatial sequence $x_n(i)$ at a given time n, one obtains the minimum length in which $\sigma_n(k)$ takes the same symbol ($k = i-h, i-h+1, \cdots, i, \cdots i+m$; the length j is $h+m+1$). The length j gives the domain size of the lattice point i at each time step n. From the spatiotemporal sampling through the entire lattice and many time steps, the probability that a lattice point belongs to the domain size j is obtained. For example, $Q(1) = 1$ and $Q(k) = 0$ for $k \neq 1$ for the complete zigzag pattern.

A static complexity of a pattern is measured by the following (static) pattern entropy:

$$S_p = -\sum_j Q(j) log Q(j). \tag{46}$$

(b)Pattern transition matrix and pattern dynamical entropy

The above quantifiers are not sufficient to study the dynamics of a pattern. We are required to construct the transition matrix of successive pattern evolution. The transition matrix is calculated as follows: First, compute the domain size to which a given lattice site i belongs at a time n (assume that the size is m). After a given time step, compute the domain size again at the lattice point (assume that the size is k). We call this as the transition m $\rightarrow$ k. By taking the spatiotemporal samplings, we obtain the probability of the transition

$$T(m \rightarrow k) = \text{transition from the domain with size m to that with size } k \ . \tag{47}$$

To see the dynamical complexity, a dynamical entropy of the transition is defined as follows:

$$S_d = -\sum_{i,j} Q(i) T(i \rightarrow j) log T(i \rightarrow j), \tag{48}$$

which is first introduced in the study of attractors of CA by the author [50].

The meaning of the quantity is as follows; Assume that we know that the lattice point belongs to the domain of some size. After a given time step, we again observe the size of domain to which the lattice point belongs. The mutual information gain through the observation is given by S_d.

As is easily shown, the relation $S_p \geq S_d$ holds. If a pattern is spatially complex but temporally frozen, $S_d = 0$ and $S_p > 0$. In the turbulent regime, both S_d and S_p are positive. If the transition occurs without a memory of the previous pattern (i.e., $T(i \rightarrow j) = p(j)$, independent of i), the equality $S_p = S_d$ holds.

If the pattern has a long-time memory and cannot be represented by the Markovian dynamics, the above transition matrix is no more useful. In such case, a distribution of the life-time is important to characterize the power-law-type behavior.

Power spectra in space or time

The spatial power spectra are defined by

$$S(k) = << |(1/N) \sum_{j=1}^{N} x_n(j) e^{2\pi i k j}|^2 >>; \tag{49}$$

where $<< *** >>$ shows the long time average.

Temporal power spectra are the power of Fourier transform of a time series of $x(i)$:

$$P(\omega) = << |(\sum_{n=t_0}^{t_1} x_n(j) e^{2\pi i n \omega}|^2 >> \tag{50}$$

These are traditional characterizations of space/time data.

References

[1] K. Kaneko, Prog. Theor. Phys. 72 (1984) 480, 74 (1985) 1033 in *Dynamical Problems in Soliton Systems* (Springer, 1985, ed. S. Takeno) 272-277

[2] K. Kaneko, Ph. D. Thesis *Collapse of Tori and Genesis of Chaos in Dissipative Systems*, 1983 (enlarged version is published by World Sci. Pub., 1986)

[3] K. Kaneko, Physica 34D (1989) 1

[4] K. Kaneko, Physica 35D (1989) in press

[5] J. P. Crutchfield and K. Kaneko,"Phenomenology of Spatiotemporal Chaos", in *Directions in Chaos* (World Scientific, 1987)

[6] I. Waller and R. Kapral, Phys. Rev. 30A (1984) 2047; R. Kapral, Phys. Rev. 31A (1985) 3868

[7] K. Kaneko, Physica 23D (1986) 436

[8] K. Kaneko, Phys. Lett. 125 A (1987) 25;Eur. Phys. Lett., 6 (1988) 193

[9] T. Yamada and H. Fujisaka, Prog. Theor. Phys. 72 (1984) 885; 74 (1985) 918:

[10] J. D. Keeler and J. D. Farmer, Physica 23D (1986) 413

[11] K. Kaneko"Phenomenology and Characterization of Spatio-temporal Chaos" in *Dynamical Systems and Singular Phenomena* (World Sci. Pub., 1987, ed. G. Ikegami)

[12] F. Kaspar and H.G. Schuster, Phys. Lett. 113A (1986) 451; Phys. Rev. A36 (1987) 842:

[13] K. Kaneko, Phys. Lett. 111A (1985) 321

[14] R.J. Deissler and K. Kaneko, Phys. Lett. 119A (1987) 397

[15] R. J. Deissler, Phys. Lett. 120A (1987) 334

[16] G.L. Oppo and R. Kapral, Phys. Rev. A33 (1986) 4219; Phys. Rev. A 36 (1987) 5820; Physica 23 D (1986) 455: R. Kapral, G.L. Oppo and D.B Brown, Physica 147 A (1987) 77

[17] I.S. Aronson, A.V. Gaponov-Grekhov, and M.I. Rabinovich, Physica 33D (1988) 1:

[18] for open flow models see also:
J.Brindley and R.M. Everson, Phys. Lett. A 134 (1989) 229:
D. Rand and T. Bohr, preprint (1988):

[19] M. H. Jensen, Phys. Rev. Lett. 62 (1989) 1361:

[20] see also H. Chate and P. Manneville, C.R. Acad. Sc. 304 (1987) 609; Phys. Rev. Lett. 58 (1987) 112

[21] H. Chate and P. Manneville, Physica 32D (1988) 409; Phys.Rev. A38 (1988) 4351; Europhys. Lett. 6 (1988) 591

[22] J.P. Crutchfield and K. Kaneko, "Space-time Information Theory", in preparation

[23] J.P. Crutchfield and K. Kaneko, Phys. Rev. Lett. 60 (1988) 2715 and in preparation

[24] L.A. Bunimovich and Ya.G. Sinai, Nonlinearity 1 (1989) 491:

[25] K. Kaneko,"Self-consistent Perron Frobenius Operator for Spatiotemporal Chaos" (LA-UR-89-1088), Phys. Lett. A, in press

[26] M. H. Jensen et al., private communication

[27] Y.Oono and S. Puri, Phys. Rev. Lett. 58 (1986)836; Phys. Rev. 38 A (1988) 1542

[28] H. Nishimori and T. Nukii, J. Phys. Soc. Jpn. 58 (1989) 563

[29] K. Kaneko, unpublished (1987)

[30] T. Bohr and M.H. Jensen, private communication

[31] J. Crutchfield, private communication (1988)

[32] R. Shaw,"boiling chaos" (movie presented at the conf. on Spatiotemporal Chaos, Los Alamos 1986):

[33] P. Alstrom and R. K. Ritala, Phys. Rev. 35A (1987) 300: H. Daido, Prog.Theor. Phys. 75 (1986) 1460:

[34] S. Coppersmith, Phys. Rev. 38 A (1988) 375

[35] K. Kaneko, talk at "the First International Conference on Form "(1986) (Tsukuba)

[36] K. Aoki and N. Mugibayashi, Phys. Lett. 128A (1988) 349:

[37] M. Rotenberg, Physica 30D (1988) 192:

[38] G. Mayer-Kress and K. Kaneko, J. Stat. Phys. 54 (1989) 1489

[39] P. Grassberger, preprint (1987)"Lumped and Distributed dynamical systems"

[40] for an application of CML to Hamiltonian systems (symplectic map lattices) see
R. Levi et al., J. Stat. Phys. 46 (1987) 147
K. Kaneko and T. Konishi, J. Phys. Soc. Jpn. 56 (1987)2993: preprint (1988)
H. Kanz and P. Grassberger, J. of Phys. A 21 (1988) L127:

[41] for CML see also;
T. Bohr et al., Phys.Rev. Lett. 58 (1987) 2155:
N.H. Packard, private communications (1986):
G. Grinstein, preprint(1988):
L.A. Bunimovich, A. Lambert, and R. Lima, preprint (1989)
T. Bohr and O.B. Christensen, preprint (1989)

[42] P.Hadley and K. Wiesenfeld, Phys. Rev. Lett. 62 (1989) 1335

[43] K. Kaneko, preprint (1989, LA-UR-89-698) K. Kaneko, preprint "Clustering, Coding, Switching, and Hierarchical Ordering in Network of Chaotic Elements"

[44] *Theory and Applications of Cellular Automata*, ed. S. Wolfram, (World Sci. Pub., 1986)

[45] J.E. Hopcroft and J.D. Ullman, *Introduction to Automata Theory, Languages, and Computation*, (Addison Wesley, 1979)

[46] U. Frisch, B. Hasslacher, and Y. Pomeau, Phys. Rev. Lett. 56 (1986) 1505; see also Complex Systems, (1987) No.4

[47] S. Aubry, in *Solitons and Condensed Matter Physics*, ed. A.R. Bishop and T. Schneider (Springer, N.Y., 1978)

[48] P. Bak, Rep. Prog. Phys. 45 (1982) 587

[49] K.Kawasaki, in *Phase Transitions and Critical Phenomena*, vol.2, ed. C. Domb and M.S. Green (Academic Press, London, 1972);

[50] K. Kaneko, in *Theory and Applications of Cellular Automata* pp. 367-399 (World Scientific, 1986, ed. by S. Wolfram)

[51] K. Kaneko, Prog. Theor. Phys. 69 (1983) 1477

[52] Y. Aizawa, I. Nishikawa, and K. Kaneko, in preparation

[53] P. Grassberger, Physica 10D (1984) 52

[54] C. Grebogi, E. Ott, and J. A. Yorke, Phys. Rev. Lett. 48 (1982) 1507; 57 (1986) 1284; Physica 7D (1983) 181

[55] C. Grebogi, E. Ott, and J. A. Yorke, to appear in Phys. Rev.A

[56] This high-dimensional crisis picture may be related with the homoclinic excursions in high-dimensional systems: A.C. Newell, D.A. Rand, and D. Russel, preprint

[57] Y. Aizawa, C. Murakami, and T. Kohyama, Prog. Theor. Phys. 79 (1984) 96

[58] I. Procaccia and H. Schuster, Phys. Rev. A28 (1983) 1210, B.C. So, N. Yoshitake, H. Okamoto and H. Mori, J. Stat. Phys. 36 (1984) 367

[59] Y. Pomeau and P. Manneville, Comm. Math. Phys. 74 (1980) 189

[60] S.P. Obukhov, Physica 101A (1980) 145: see Y. Pomeau, Physica 23D (1986) 3, for a suggestion on the relation with intermittency.

[61] K. Kaneko and Y. Akutsu, J. Phys. A19 (1986) L69-74

[62] S. Nasuno, M. Sano, and Y. Sawada, in *Cooperative Dynamics in Complex Systems* (Springer, 1989, ed. H. Takayama) and private communications

[63] M.J. Feigenbaum, J. Stat. Phys. 21 (1979) 669

[64] F. Heslot, B. Castanig, and A. Libchaber, Phys. Rev. A 36 (1987) 5870

[65] L.D. Landau and E.M. Lifshitz, *Fluid Mechanics* (Pergamon, London, 1959) Chapt.3

[66] D. Ruelle and F. Takens, Comm. Math. Phys. 20 (1971) 167, 23 (1971) 343

[67] R. Shaw, Z. Naturforshung, 36a (1981) 80; *The Dripping Faucet as a Model Chaotic System*, (Aerial Press, Santa Cruz, 1984)

[68] R. Bowen and D. Ruelle, Inventiones Math. 29 (1975) 181; D. Ruelle, *Thermodynamic Formalism*, Addison Wesley, Reading, MA (1978)

[69] Y. Oono, Prog. Theor. Phys. 60 (1978) 1944; Y. Oono and Y. Takahashi, Prog. Theor. Phys 63 (1980) 1804.

[70] T. Kai and K. Tomita, Prog. Theor. Phys. 64 (1980) 1532

[71] H. Mori, B-C. So and T. Ose, Prog. Theor. Phys (1981) 1266

[72] H. A Gutowitz, J.D. Victor, and B.W. Knight, Physica 29D (1987) 18; H. A. Gutowitz and J. D. Victor, J. Stat. Phys. 54 (1989) 495

[73] Y. Oono and C. Yeung J. Stat. Phys. 48 (1987) 593; see also, Y. Oono and M. Kohmoto, Phys. Rev. Lett. 55 (1985) 2927

[74] J. S. Langer, M. Bar-On, and H.P. Miller, Phys. Rev. A 11 (1975) 1417

[75] Y. Kuramoto and T. Tsuzuki, Prog. Theor. Phys. 55 (1976) 356

[76] see for the approach with CA and temperature field, N. H. Packard, in *Theory and Applications of Cellular Automata* (World Scientific, 1986, ed. by S. Wolfram)

[77] J. Nagumo and S. Sato, Kybernetik 10 (1972) 155

[78] L.D. Harmon, Kybernetik 1 (1961) 89

[79] P. Bak, C. Tang, and K. Wiesenfeld, Phys. Rev. Lett., 59 (1987) 381

[80] H. Hayashi et al., Phys. Lett. 88 A (1982) 265

[81] K. Aihara and G. Matsumoto, in *Chaos* (ed. A.V. Holden, Princeton, 1986)

[82] W. Freeman and C. A. Skarda, Brain Res. Rev. 10 (1985) 147; W. Freeman, Brain Res. Rev. 11 (1986) 259; Biol. Cybernetics 55 (1987) 1;

[83] M. Mezard, G. Parisi, and M.A. Virasoro eds., *Spin Glass Theory and Beyond* (World Sci. Pub. 1987)

[84] L.N. Cooper, in *Proc. of Nobel Symposium on Collective Properties of Physical Systems*, B. Lundruist and S. Lundruist eds. (1973, Academic Press)

[85] W.A. Little and G.L. Shaw, Behavioral Biology 14 (1975) 115

[86] J. J. Hopfield, Proc. Natl. Acad. Sci. 79 (1982) 2554

[87] Y. Kuramoto, *Chemical Oscillations, Waves, and Turbulence*, Springer, 1984

[88] G.B. Ermentrout and N. Kopell, SIAM J. Math. Anal. 15 (1984) 215; N. Kopell and G.B. Ermentrout , in *Nonlinearity in Biology and Medicine*, (eds A.S. Perelson, B. Goldstein, M. Dembo,and J.A. Jacquez, Elsevier, 1988)

[89] *Spatiotemporal Coherence and Chaos in Physical Systems*, (North Holland, ed. A. R. Bishop, G. Gruner, and B. Nicholaenko, 1986)

[90] T. Ikegami and K. Kaneko, to be published

[91] A. T. Winfree, in *Oscillation and Traveling Waves in Chemical Systems*, ed. R.J. Fields and M. Burger (John Wiley and Sons, 1985): see also Y. Kuramoto, *Chemical Oscillations, Waves and Turbulence*, (Springer, N.Y., 1984) for theoretical stage.

[92] H. Yamazaki, Y. Oono and K. Hirakawa, J. Phys. Soc. Jpn. 44 (1978) 335

[93] G. Ahlers and R. P. Behringer, Prog. Theor. Phys. 64 (1978) 186

[94] E. Moses and V. Steinberg, Phys. Rev. Lett.57(1986) 2018

[95] S. Ciliberto and M. A. Rubio, Phys. Rev. Lett. 58 (1987) 2652

[96] R.W. Walden, P. Kolodner, A. Passner, and C.M. Surko, Phys. Rev. Lett. 55 (1985) 496

[97] S. Sato, M. Sano and Y. Sawada, private communication

[98] R. J. Donnelly et al., Phys. Rev. Lett. 44(1980) 987: G. W. Baxter and C. D. Andereck, Phys. Rev. Lett 57(1986) 3046

[99] S. Ciliberto and J.P. Gollub, Phys. Rev. Lett. 52 (1986) 922

[100] S. Kai and K. Hirakawa, Prog. Theor. Phys. Suppl. 64 (1978) 212

[101] M. Lowe, J. P. Gollub and T. C. Lubensky, Phys. Rev. Lett. 51(1983) 786

[102] R. V. Buskirk and C. D. Jeffries , Phys. Rev. A 31 (1985) 887

[103] A. Zettl, Physica 23D (1986) 155

[104] see e.g., K. R. Sreenivasan, in *Frontiers of Fluid Mechanics*, (Springer, 1985, eds. by S.H. Davis and J.L. Lumley)

[105] see e.g., J.J. Riley and M. Gad-el-Hak, in *Frontiers of Fluid Mechanics*, (Springer, 1985, eds. by S.H. Davis and J.L. Lumley)

[106] M. Donetti, R. Meynart, J.P. Boon, and D. Olivari, Phys. Rev. Lett. 55 (1985) 492

[107] Y. Sawada, Physica 140A (1986) 134

[108] S. Ciliberto and P. Bigazzi, Phys. Rev. Lett. 60 (1988) 286